5-9-2014

Target Species Selection for Dynamic Adaptive Chemistry Simulations

Nicholas Curtis
nicholas.curtis@uconn.edu

Target Species Selection for Dynamic Adaptive Chemistry Simulations

Nicholas Curtis

B.Eng., McGill University, 2012

A Thesis

Submitted in Partial Fulfillment of the

Requirements for the Degree of

Master of Science

At the

University of Connecticut

2014

APPROVAL PAGE

Masters of Science Thesis

Target Species Selection for Dynamic Adaptive Chemistry Simulations

Presented by

Nicholas Curtis, B.Eng.

Major Advisor_____
Dr. Chih-Jen Sung

Associate Advisor_____
Dr. Tianfeng Lu

Associate Advisor_____
Dr. Baki M. Cetegen

University of Connecticut

2014

Acknowledgements

I would like to thank Dr. Chih-Jen Sung for providing me with the opportunity to take on challenging, complex problems in a field that continually excites me, as well as for his invaluable support and instruction.

Additionally, I would like to thank Kyle Niemeyer for his help with reviewing and proofing this document.

I would also like to thank my parents for all their support through this process and for their efforts to introduce me to wonderfully disparate fields of math and science at a young age.

In addition, I would also like to thank the other members of the Combustion Diagnostics Laboratory for their advice and support.

Finally, I would like to thank my friend Mike Sanchick, who completely changed my life for the better the day we began to talk about music.

Contents

Target Species Selection for Dynamic Adaptive Chemistry Simulations

Abstract

By

Nicholas Curtis

The Relative Importance Index (RII) method for determination of appropriate target species for dynamic adaptive chemistry (DAC) simulations using the directed relation graph with error propagation (DRGEP) method was developed and validated for two fuels, n-heptane and isopentanol, which are representatives of a ground transportation fuel component and a bio-alcohol, respectively. The conventional method of DRGEP target species selection involves picking an unchanging (static) set of target species based on the expected major combustion processes; however, these static target species may not remain important throughout a combustion simulation. The RII method determines appropriate DRGEP target species solely from the local thermochemical state of the simulation, enabling DAC simulations to better respond to changing combustion conditions while ensuring that accuracy will be maintained. Further, the RII method reduces the expertise required of users to select DRGEP target species sets appropriate to the combustion phenomena under consideration. The RII method was tested on constant volume ignition delay studies as well as single-cell engine simulations under homogenous charge compression ignition (HCCI) conditions for n-heptane and isopentanol reaction mechanisms. It is illustrated that the RII is capable of accurate predictions of constant volume ignition delays over a wide range of starting conditions. Further, for a similar maximum error in ignition delay predictions, under certain autoignition conditions the RII method produced considerably smaller local skeletal mechanisms compared to those of conventional DRGEP target species selections; however, both methods generated

similarly sized local skeletal mechanisms outside these regions. In addition, the RII method was capable of accurately predicting ignition crank angles for single cell engine simulations under HCCI conditions with significantly smaller local skeletal mechanisms than conventional DRGEP target species selections.

1. Introduction

1.1 Role of Combustion in Society

Combustion of fossil fuels is incredibly important to the supply of energy in the United States. Fossil fuel combustion has provided 87% of total primary energy over the last decade, and is projected to supply more than 75% of the nation's primary energy demand in 2040 [1]. Additionally, combustion-related carbon dioxide emissions account for more than 80% of United States' greenhouse gas emissions [2]. More efficient, reduced pollutant emission combustion solutions are a necessity to supply national energy demand while meeting increasingly stringent carbon dioxide and pollutant emissions limits.

It is estimated that a 30–50% reduction in fuel consumption in light-duty vehicles (i.e. passenger cars) can be achieved over the next 30 years [3]. In the near term the bulk of this reduction will occur through development and implementation of advanced internal combustion engines. In addition, the ACARE Flightpath 2050 plan [4] calls for a 30% reduction in airplane CO_2 emissions and a 90% reduction in NO_2 emissions, resulting from improved gas turbine technology. In order to achieve these goals engineers have begun exploring new combustion schemes such as low-temperature combustion (LTC), which achieves high efficiency and low emissions via the high compression ratio combustion of either very dilute or fuel lean mixtures. Computational combustion modeling is an important tool used increasingly to investigate and develop novel combustion devices [5-11], and has demonstrated an ability to aid in and speed up the design-cycle of next generation combustion devices. However, a number of problems exist that limit its practicality.

1.2 Barriers to Computational Combustion Modeling

Detailed, accurate chemical models are a necessity in order to accurately predict combustion phenomena in high-fidelity simulations of both advanced transportation engines and gas turbines [6, 12]. Traditionally, engine designers have utilized greatly simplified reaction mechanisms containing only a few species and reaction steps to capture fuel breakdown and heat release. These simplified global

mechanisms typically are only applicable in a narrowly defined set of combustion conditions; a problem in practical combustion applications where a variety of different combustion modes are observed [13].

In order to achieve high efficiencies and low emissions, new engine types using novel combustion regions, such as LTC, are being investigated and developed. One method of achieving LTC is the homogenous charge compression ignition (HCCI) approach, in which a highly homogenous mixture is burned at very fuel-lean conditions and high compression ratios. The high compression ratios allow HCCI combustion to reach the efficiency of diesel engine; high fuel concentrations responsible for soot and NO_x emissions are avoided however, resulting in orders of magnitude less pollutant emissions [14] than diesel engines. The very lean mixtures typically utilized in HCCI combustion tend not to propagate like an ordinary flame; as such ignition timing is very sensitive to fuel chemistry and local conditions [15]. As a result, HCCI combustion is primarily controlled by chemical kinetics, and thus accurate chemical models are required for high fidelity predictions.

Modeling of gas turbine technology is another area where detailed chemical kinetics models are required. Lean premixed combustion has proven to be very successful in reducing nitrous oxide (NO_x) emission levels; however, detailed chemistry is still required to accurately predict the ignition delay [16] as well as NO_x formation, unburned hydrocarbon, and pollutant levels [12, 17]. Additionally, complex gas turbine phenomena such as lean blowout, a cause of expensive shutdown/restart cycles in power generation turbines and a major safety hazard for aerospace applications, often require the use detailed chemistry. For example, in order to accurately predict extinction strain rates, a necessity for high-fidelity simulation of local flame extinction events (which in turn can cause lean blowout [18]), the use of detailed chemical models is required [13, 16].

Over time, the need for accurate chemical reaction mechanisms has been recognized, resulting in the development of more detailed and complex chemical kinetic models for transportation fuels. For instance, a recently proposed gasoline surrogate mechanism [19] contains approximately 1550 different chemical species and 6000 reactions, while a recent biodiesel surrogate mechanism [20] contains around

3300 species and over 10000 reactions. The large size of these mechanisms makes them expensive even for use in simple zero-dimensional combustion studies due to the problem of chemical stiffness.

Chemical stiffness is induced by quickly depleted radicals reaching a quasi-steady state and fast reversible reactions in partial equilibrium, causing species and reaction time scales to range from nanoseconds to seconds [13]. Large hydrocarbons typically have high levels of chemical stiffness, making use of explicit integration algorithms inefficient; instead implicit integration algorithms must be utilized [13]. However, implicit integration typically requires the factorization of a non-sparse Jacobian matrix, an operation that scales cubically in cost with the number of species in a mechanism [13]. The high cost of implicit chemical integration is such that even in some cases utilizing a relatively small chemical mechanism (e.g. ~50 species), chemical integration can consume between 75-99% of total computational time in a multi-dimensional reacting flow simulation [21-23]. In order to utilize large, complex chemical mechanisms relevant to transportation and energy fuels in realistic, useful simulations, accurate mechanism reduction and chemical stiffness removal strategies must be employed.

1.3 Mechanism Reduction Techniques

1.3.1 Reaction State Sampling

When reducing chemical mechanisms from detailed chemical models to a much smaller size suitable for use in larger scale simulations, the range of validity is a very important consideration. A comprehensive mechanism is generated by sampling reaction states from a range of thermochemical conditions, known as a thermochemical state space. A comprehensive mechanism is expected to be valid over the entire thermochemical state space. Although use of comprehensive mechanism for conditions outside the thermochemical state space from which it was generated can result in large errors [13], comprehensive mechanisms generated from broad thermochemical state spaces can often be applied to more general state spaces (e.g., those of multi-dimensional simulations) with satisfactory accuracy [24]. In contrast, a local mechanism is generated from and can only be assumed to be valid at one

thermochemical state; use of a local mechanism at any state other than the one for which it was generated is likely to induce large error.

1.3.2 Time Scale Analysis

The first major category of mechanism reduction methods employs chemical time-scale analysis to reduce chemical stiffness by removing short time scales caused by rapidly depleted species and fast reversible reactions. The classical Quasi-Steady State approximation (QSS) [25] and the Partial Equilibrium approximation (PE) [26, 27] were among the first methods of time-scale reduction. By assuming that QSS species rapidly reach a quasi-steady state, their concentrations can be expressed as a set of algebraic equations instead of differential equations. Similarly, the PE approximation assumes that a reaction quickly reaches a partial equilibrium after initial transience. Methods such as such as computational singular perturbation (CSP) [28-30] and intrinsic low-dimensional manifolds (ILDM) [31] are more systematic time-scale analysis methods; using Jacobian analysis the fast and slow reaction modes are decoupled to reduce chemical stiffness. Offshoots of these approaches can also be used to identify QSS species and PE reactions [32, 33]. As these methods typically require Jacobian analysis, the cost of which scales cubically with the number of species, their use on large chemical mechanisms can be expensive.

1.3.3 Skeletal Mechanism Reduction

The second major category of mechanism reduction techniques attempts to remove species and reactions that are deemed non-important to the detailed chemical mechanism over a specified range of interest (e.g., temperature, pressure, and equivalence ratio). Sensitivity analysis [34-36] is a classical skeletal reduction method that identifies and eliminates unimportant reactions and species via analysis of the Jacobian matrix. An offshoot of sensitivity analysis, principal component analysis [37] determines a number of primary ‘coordinates’ of the sensitivity matrix, giving information about species and reaction coupling which is then used to identify unimportant species and reactions. Additionally, CSP-based methods can be adapted for use in skeletal mechanism reduction; species strongly coupled in either the

fast or slow subspaces are considered important and are kept in the skeletal mechanism [38-40]. A similar method called level of importance analysis (LOI) combines time-scale analysis with sensitivity analysis in order to rank species importance [41-44], and thus determine unimportant species. The previously described methods rely on Jacobian/Sensitivity matrix analysis, and thus their cost scales cubically with the number of species under consideration, a problem for large mechanisms.

Other methods include genetic algorithms [45, 46] and optimization methods [47-49]. Genetic algorithms take inspiration from natural selection, attempting to find the subset of species that best matches combustion targets through trial and error of successive generations of skeletal mechanisms. Optimization methods use linear-programming theory to eliminate species and reactions while meeting combustion targets within a specified error limit. Although these methods can produce highly compact skeletal mechanisms, they are classified as NP-Hard, meaning that cost of finding the true optimal solution scales exponentially with the number of species in the mechanism.

The directed relation graph (DRG) method proposed by Lu and Law [50] has been extensively used to efficiently and reliably produce skeletal mechanisms from large starting mechanisms [51]. First, a graph with edges representing inter-species coupling is created. A graph search is then started from a selected set of target species; species only weakly coupled to these targets are considered unimportant and are removed from the resulting skeletal mechanism. Since its inception, the DRG method has been extended in several different directions; DRG-aided sensitivity analysis (DRGASA) performs sensitivity analysis on species not removed during the DRG step [52] to generate even more compact skeletal mechanisms, while the DRG with error propagation (DRGEP) method [53], considers the effect of error propagation due to species removal along graph pathways. The DRGEP and DRGASA methods were further adapted into the DRGEPSA method [54, 55], which was found to generate more compact skeletal mechanisms than either the DRG, DRGEP, or DRGASA methods at the same level of accuracy. As the DRGEP method is a key component of this work, the subsequent sections will examine the DRG and DRGEP methods in detail.

1.3.3.1 Directed relation Graph Method

The directed relation graph method, original proposed by Lu and Law [50-52], uses a directed graph to map species coupling as edges between vertices on the graph. Species are considered unimportant and are removed from the skeletal mechanism if a path connecting them to a specified set of target species cannot be found. The DRG method maps each species in the mechanism to a vertex on the graph; there is a directed edge between species *A* and *B* if and only if $r_{AB}^{DRG} \geq \varepsilon_{DRG}$, where

$$r_{AB}^{DRG} = \frac{\sum_{i=1}^{N_R} |\nu_{A,i}\omega_i\delta_{B,i}|}{\sum_{i=1}^{N_R} |\nu_{A,i}\omega_i|} \quad (1)$$

$$\delta_{B,i} = \begin{cases} 1 \; if \; reaction \; i \; involves \; species \; B \\ 0 \; otherwise \end{cases} \quad (2)$$

$\nu_{A,i} = \nu''_{A,i} - \nu'_{A,i}$ is the net stoichiometric coefficient of species *A* in reaction *i*, ω_i is the net reaction rate N_R the total number of reactions in the mechanism, and ε_{DRG} is a small cutoff threshold (e.g. 0.1), referred to as the DRG cutoff.

The r_{AB}^{DRG} value, also known as the direct interaction coefficient (DIC), attempts to quantify the dependence of the of species *A* on species *B*. We can say that if r_{AB}^{DRG} is large then the activity of species *A* is strongly dependent on species *B*. Therefore, if species *A* is kept in the resulting skeletal mechanism, species *B* should be kept as well.

The DRG is then utilized to generate a skeletal mechanism as follows; first, a set of starting vertices, also known as target species or search initiating species, are selected. A depth-first search is initiated at these starting vertices; the set of species reached by the graph search are considered to be important to the overall production of the target species, and are therefore kept in the resulting skeletal mechanism. A simplified example of this reduction procedure is pictured in Fig. 1.

While the DRG cutoff ε_{DRG} can be specified directly by the user, for comprehensive skeletal mechanism generation it is preferable to determine it iteratively to ensure strict error control. The procedure for this is as follows; first a thermochemical state space is created by sampling reaction states

from a variety of relatively simple combustion problems (e.g. constant volume ignition, perfectly stirred reactors, etc.), in addition combustion targets for these problems (e.g. ignition delay, extinction residence time, key species mass fractions) are determined. Starting from a very low DRG cutoff (e.g. 10^{-3}), a comprehensive skeletal mechanism is generated from the defined state space by taking the union of a local skeletal mechanism generated for each point in the state space. The resultant comprehensive skeletal mechanism is then tested on the same simple combustion problems and the error in combustion targets is determined. The DRG cutoff is then raised and the procedure repeated until the error in combustion targets resulting from use of the skeletal mechanism is no longer below a user specified limit.

The target species set for a DRG reduction can simply consist of the fuel, through which the oxidizer as well as important radicals are included [50]. If accuracy is required for additional phenomena (e.g. NO_x predictions), a corresponding species (i.e. NO) should also be included in the target set [50]. Finally, in the DRG method species that only participate as third bodies in reactions are not considered to be involved in the reaction (Eq. 1-2). Therefore inert species can be included in the target set, such that they are not removed from the resultant skeletal mechanism.

1.3.3.2 Directed relation Graph with Error Propagation Method

The directed relation graph with error propagation (DRGEP) method, originally proposed by Pepiot-Desjardins and Pitsch [53], is an extension of the original DRG method that considers the propagation of error caused by species removal down reaction pathways. Motivated by shortcomings of the original DIC definition [50] in situations with long chemical paths involving fast modes [56] the DRGEP method uses a modified definition of the direct interaction coefficient:

$$r_{AB}^{DRGEP} = \frac{\left|\sum_{i=1}^{N_R} \nu_{A,i}\omega_i\delta_{B,i}\right|}{\max(P_A, C_A)} \tag{3}$$

where

$$P_A = \sum_{i=1}^{N_R} \max(0, \nu_{A,i}\omega_i) \tag{4}$$

$$C_A = \sum_{i=1}^{N_R} \max(0, -\nu_{A,i}\omega_i) \tag{5}$$

$$\delta_{B,i} = \begin{cases} 1 \; if \; reaction \; i \; involves \; species \; B \\ 0 \; otherwise \end{cases} \tag{6}$$

Unless otherwise specified, the direct interaction coefficient r_{AB} will be assumed to be the DRGEP direct interaction coefficient r_{AB}^{DRGEP} from this point on.

A path dependent interaction coefficient (PIC) from the set of target species is then defined on the path p from a target species T_j to species *B* as:

$$r_{T_jB,p} = \prod_{i=1}^{length(p)-1} r_{S_iS_{i+1}} \tag{7}$$

where the ith edge of path p connects species S_i and S_{i+1}. The interaction coefficient for target T_j is defined as the maximum of all PICs between T_j and B:

$$R_{B,j} = \max_{all \; paths \; p} (r_{T_jB,p}) \tag{8}$$

Finally, the overall interaction coefficient (OIC) is defined as:

$$R_B = \max_{T_j \in targets} R_{B,j} \tag{9}$$

The species *B* is then considered active in the mechanism if and only if:

$$R_B \geq \varepsilon_{DRGEP} \tag{10}$$

where $\varepsilon_{\mathrm{DRGEP}}$ is a small cutoff threshold (e.g. 10^{-4}), which will be referred to as the DRGEP cutoff.

Similar to the DRG method, the DRGEP DIC r_{AB} is intended to estimate the error in overall production or consumption of species *A* induced by the removal of species *B* from the mechanism. The PIC $r_{T_jB,p}$ captures the propagation of this error down the pathway *p* from a target to species *B*. By

taking the OIC R_B to be the maximum PIC value for B from all targets, a reasonable estimate of the error induced on the target species by removal of species *B* is obtained. Fig. 2 shows an sample reduction using the DRGEP method.

The DRGEP method can be viewed as a more aggressive version of the DRG method. If some error is introduced by removal of species *B* from the skeletal mechanism, this error must propagate to reach the target species *A*; a species further away on the graph from the target set is more likely to be removed than in the DRG method for this reason. As a result the DRGEP method is much more sensitive to the selection of target species; the effect of different target species sets on the DRGEP method will be investigated in greater detail in Chapter 2.

Following the work of Niemeyer and Sung [57], Dijkstra's algorithm was used to perform the graph search to determine the OICs. In order to improve execution speed in a dynamic adaptive chemistry (DAC) context, modifications were made to the search algorithm such that only a single graph search (including all target species) is performed and unnecessary graph edges are not expanded. Full pseudo code is detailed in Appendix A.

1.3.4 Compact Comprehensive Mechanism Generation

Often when generating a comprehensive skeletal mechanism, several mechanism reduction techniques are applied in sequence to generate the most compact mechanism possible. Methods commonly used to further reduce comprehensive skeletal mechanisms are species lumping [52, 58-60], error cancellation [61], and unimportant reaction elimination [52]. Isomer lumping attempts to treat similar chemical species in the reaction mechanism (e.g. chemical isomers) as a single species in order to reduce the number of variables in the system, resulting in accelerated computation. Error cancellation attempts to identify pairs of species whose removal from the mechanism induces error of similar magnitude, but with opposite signs. By removing both species at once, the induced errors tend to cancel leaving a reduced system with minimal induced error. Finally, in the unimportant reaction elimination method, a reaction is considered unimportant (and removed from the skeletal mechanism) if the

maximum of its normalized contributions to all species is less than a threshold value $\varepsilon_{\mathrm{reac}}$ which can either be user specified, or determined iteratively based on a user-specified error limit in combustion targets (e.g. ignition delay).

As seen previously, the directed relation graph with error propagation aided sensitivity analysis (DRGEPSA) method is one technique for comprehensive skeletal mechanism generation. In DRGEPSA a DRGEP reduction is applied first, before further considering sensitivity analysis to the species deemed marginally important by the DRGEP method. DRGEPSA has been found to generate more compact mechanisms than just the DRGASA or DRGEP methods alone [55]. Another work applied DRG reduction, followed by isomer lumping, DRGASA and Error Cancellation to find a 115 species comprehensive skeletal mechanism from a 3299 species detailed biodiesel mechanism [61].

1.4 Adaptive Chemistry Reduction

Comprehensive skeletal mechanisms generated based on a priori selected thermochemical states and user specified error limits are at a disadvantage in multi-dimensional simulations in that they apply the same level of detail to the entire multi-dimensional domain. Consider that inside the flame zone of a multi-dimensional simulation, a highly accurate skeletal mechanism with many species will likely be needed, but outside the flame zone a much smaller mechanism may be sufficient. Further, ensuring that a comprehensive skeletal mechanism remains accurate over the full range of conditions will likely cause the mechanism to be too large to be used in multi-dimensional simulations. These problems motivate the use of adaptive chemistry (AC), which seeks to achieve computational speedup by using only locally relevant skeletal mechanisms.

Given a starting chemical mechanism, AC simulations pre-generate a number of skeletal mechanisms based on expected thermochemical conditions. During the simulation an appropriate locally relevant skeletal mechanism is chosen based on the local thermochemical state. The full chemical state is

mapped to the skeletal mechanism and integrated; the results are mapped back to the full mechanism and stored for the next simulation time step.

One of the first uses of AC [62] switched between H_2/O_2 mechanisms simply based on hydrogen and oxygen mass fractions. Although the adaptive scheme was able to reproduce species profiles in a planar reacting shear layer, little speedup was achieved due to the small size of the starting mechanism. A later paper from Banerjee et al. [63] used genetic algorithms to produce skeletal mechanisms starting from the GRI 3.0 mechanism [64], and further to identify the valid thermochemical range of application for each skeletal mechanism. Although the scheme was able to accurately predict temperature and species traces in a pairwise mixed stirred reactor (PMSR) simulation, it is noted that the use of genetic algorithms to generate skeletal mechanisms from larger starting mechanisms can be quite expensive. Further, there is no guarantee that a given thermochemical state in the simulation will map to a reduced mechanism, requiring use of the detailed starting mechanism in some cases. He et al. [65] proposed a method of elemental flux clustering to group thermochemical states. After similar states were clustered into groups, a skeletal mechanism was generated for each cluster. During the simulation, the appropriate reduced mechanism was chosen based on their distance from the cluster centers. This method was capable of accurately predicting temperature and major mass fractions of an n-pentane mechanism in a PMSR simulation with a speedup of over sixty times compared to the detailed mechanism. A recent work from Liang et al. [66] used binary partitioning along principal components of the sampled thermochemical space to group thermochemical states, generating a skeletal mechanism using DRGEP for each. The approach was able to accurately match the detailed mechanism in a partially stirred reactor simulation.

Although the AC approach is capable of highly accurate predictions, often with large computational gains, there are issues with the approach. First, it relies on being able to predict the range of conditions expected to be seen in the full scale simulation. It remains an open question whether reaction state sampling from zero-dimensional homogenous simulations can explore the entire range of conditions necessary for accuracy in a multi-dimensional simulation; it is possible that diffusive systems

may also need to be sampled [13]. Further, as local extinction and ignition may be present in large scale multi-dimensional simulations, the AC approach must include skeletal mechanisms that accurately describe low-temperature ignition chemistry as well as the high-temperature flame chemistry [13]. The AC scheme is additionally limited by the number of pre-generated skeletal mechanisms. Not only is the memory occupied by these mechanisms potentially an issue, implementing an efficient high-dimensional search to find the appropriate skeletal mechanism may also be a problem. In a study from Liang et al. [67] querying the skeletal mechanism library using a nearest neighbor search was found to incur significant computational overhead.

When the AC scheme encounters unmapped thermochemical states a variety of potential sub-optimal solutions may be taken. First, the unmapped state may be assigned to the 'closest' skeletal mechanism (as determined by one of the previously described selection methods). However, this may induce large error if the skeletal mechanism is not truly applicable. Further consider that unmapped reaction states may correspond to unexpected or undesirable behavior of the combustion system; taking this option, though simple, may actually induce large error in interesting phenomena. A second option is to simply use the full detailed mechanism when unexpected states are encountered, yet the size of the detailed mechanism is the main motivation for an adaptive chemistry scheme to begin with; if the detailed mechanism is large and unexpected states are encountered with any frequency, this solution may be computationally prohibitive. The last option is to simply generate a new skeletal mechanism for use with the unexpected state; depending on the type of mechanism reduction utilized, this may be a costly step in its own right. Further concerns may include the memory requirements for storage of additional mechanisms, as well as potentially increasing the cost of searching for the appropriate skeletal mechanism for future states.

1.5 Dynamic Adaptive Chemistry Reduction

In order to address the issues with the adaptive chemistry scheme, Liang el al. [68, 69] developed a method known as dynamic adaptive chemistry (DAC). In a DAC simulation a reduction method is

applied to each instantaneous thermochemical state, generating a small but only locally accurate skeletal mechanism. This locally accurate mechanism is integrated for a single simulation time step, and the resulting thermochemical state is stored. After its use, the locally accurate mechanism is discarded and the process repeats at the next simulation time step. By generating a skeletal mechanism for each thermochemical state, the DAC scheme ensures that the resulting skeletal mechanism is rigorously valid for that state; thus the problems of unexpected reaction states in the AC scheme are alleviated. However, in order for significant computational gains to be realized using DAC, the cost of skeletal mechanism generation must outweighed by the resulting speedup from integrating the smaller, locally accurate mechanism. For this reason, reduction methods that scale linearly with the problem size (e.g., DRG-based methods [50], Element Flux Analysis [70]) are typically used.

In their original DAC work, Liang et al. [68] coupled the DAC scheme to the DRGEP method. At each time step, the DRGEP method is applied to the local thermochemical state in order to determine the active species to be kept in the resultant local skeletal mechanism. Reactions are included in the skeletal mechanism only if all the reactants and products are active species (not counting third bodies). Species not in the active set are treated as inactive, and their mass fractions are kept fixed. Given a system with *m* active species (superscript *a*), *n* inactive species (superscript *i*), and a state $\boldsymbol{X}\left(T, p, y_1^a, \dots y_m^a, y_1^i, \dots y_n^i\right)$, the resulting chemical kinetic system can be described as:

$$\begin{cases} \dot{y}_1^a = f_1\left(T, p, y_1^a, \dots y_m^a, y_1^i, \dots y_n^i\right) \\ \quad \vdots \\ \dot{y}_m^a = f_m\left(T, p, y_1^a, \dots y_m^a, y_1^i, \dots y_n^i\right) \\ \dot{T} = f_{m+1}\left(T, p, y_1^a, \dots y_m^a, y_1^i, \dots y_n^i\right) \end{cases} \tag{11}$$

Although inactive species do not participate as reactants in any active reaction, their removal can induce serious error in third body reactions and pressure dependent reactions. In order to minimize the size of the ODE system while accounting for these third body effects, the DAC scheme calculates the net species production rates of the active species, as well as the derivatives of any state variables (e.g. temperature, pressure) based on the entire thermochemical state (including inactive species) as seen in Eq. 11.

The DRGEP target species set was selected to include species from the major combustion processes of HCCI combustion; the fuel (n-heptane) was selected to cover hydrocarbon decomposition pathways, HO_2 was selected to include water production (H_2-O_2 reactions), and CO was selected to include CO_2 creation pathways (primarily through CO oxidation). Using this target species set and a DRGEP cutoff value $\varepsilon_{DRGEP} = 10^{-4}$, a 30 fold speed up was achieved for a single cell HCCI ignition simulation using a detailed n-heptane mechanism [71], while excellent accuracy in pressure trace and species mass fractions were maintained.

A later work from Liang et al. [69] extended the DAC scheme to gasoline surrogate fuel mechanisms. It was found that the target species set including n-heptane, HO_2, and CO worked well for all the studied n-heptane / isooctane / toluene blends. Further, the most reactive fuel species needed to be included in the target set, but the other fuels could be included with little impact on computational time. The DAC scheme was also able to capture the hydrocarbon/NO sensitization effect on the hydrocarbon ignition processes studied without direct inclusion of NO in the target species set. Once a target species reached very low concentrations, it was found that including it in the target species set resulted in many unimportant species being introduced back into the skeletal mechanism. To maintain computational efficiency, it was suggested that target species with mass fraction less than 10^{-30} should be removed from the target species set. The same DRGEP cutoff value of 10^{-4} worked well in all cases.

The effect of the integration time step on DAC accuracy was also studied. In the most general case for implicit integration schemes (DVODE [72] was used in this study) the Jacobian must be generated numerically and factorized, time consuming processes. Therefore to increase computational efficiency, the Jacobian is reused for multiple internal integration steps until it is deemed unsuitable. In the DAC scheme however, the Jacobian must be reinitialized at each time step, as a different chemical system is being described by each skeletal mechanism. By increasing the chemical integration time step size the same Jacobian is expected to be reused more often, and thus the simulation will be faster. However, for fast chemical problems (e.g. auto-ignition), raising the chemical integration time step was

found to induce unacceptable error as the local skeletal mechanism generated was not necessarily reliable for the entire time step. For fast chemical processes a sufficiently small time step (e.g. 10^{-5} s) must be selected to maintain accuracy.

Detailed (1099 species) and skeletal (150 species) gasoline surrogate mechanisms based on those from Andrae et al [73, 74] (modified to include NO_x formation using the GRI-3.0 sub mechanism [64]) were tested in single-cell HCCI simulations as well as in shock tube ignition delay problems. Up to a 70x and 15x speedup was found for the detailed and skeletal mechanisms respectively for HCCI simulations, while a 10x and 2x speedup was found for shock tube ignition delay timings.

He et al. [70] paired an element flux analysis method with the DAC scheme to study n-pentane combustion. The method was able to accurately predict the combustion of n-pentane in a pairwised mixed stirred reactor (PMSR) with a speedup factor of approximately 25. The method was then tested on adiabatic plug flow reactor auto-ignition predictions. Although a speedup over two times was achieved for the n-pentane mechanism, it is noted that the cost of the element flux method reached up to 20% of total computational time.

Yang et al. [75] paired the DAC scheme with the DRG method for turbulent methane flame simulations. They found that the DAC approach was capable of accurately reproducing the combustion process of a partially stirred reactor simulation (PaSR) with a significant level of non-equilibrium processes. Further the computationally optimal way of operating the DAC scheme when the chemical integration time step was larger (e.g. 10^{-4} s or longer) than the timescale of validity (e.g. 10^{-5} s [69]) of the local skeletal mechanism was investigated; it was found that generating a skeletal mechanism with a longer applicable timescale, e.g. by lowering the DRG cutoff, from $\varepsilon_{DRG} = 0.1$ to a smaller value — 0.01 or 0.001, was more efficient than performing multiple DRG reductions within each chemical integration time step. The DRG based DAC scheme achieved a speedup factor of two to four for non-premixed cases using the USC-Mech II [76] and two to six for premixed cases with good accuracy in temperature and species concentrations; with the GRI-Mech 3.0 [64] the DAC scheme achieved a speed factor up to three.

Tosatto et al. [77] formulated a DRG based DAC scheme that took into account transport fluxes, and applied it to several flame simulations. A speedup factor of 5 was reported for a steady JP-8 flame, while a larger speed up factor of 10 was found for a time dependent ethylene flame. The distribution of active species numbers kept in the mechanism was found to closely mirror the spatial structure of the flame itself.

Gou et al. [78] paired a simplified version of the path flux analysis method [79] with the DAC scheme in an effort to address the challenge of controlling error in a DAC scheme. First a table of threshold values was determined such that accuracy was maintained for key parameters (e.g. temperature, pressure, major species mass fractions) in homogenous ignition studies. During the simulation, the optimal cutoff value was determined via the look-up table based on the local conditions and a reaction progress variable in order to generate the local skeletal mechanism. The error controlled DAC scheme (EC-DAC) was capable of speedups factors from 5-100 with tight error control. It is noted however that this scheme relies on reliably predicting the range of combustion conditions that will be encountered, which is potentially a problem as seen in Section 1.4. Additionally, the selection of the reaction progress variable (mass fraction of oxygen) may not be optimal in turbulent reacting systems, where the role of mixing is much more pronounced. More investigation is needed into strict error control for DAC simulations.

Shi et al. [23] applied the DAC/DRGEP scheme to the simulation of direct injection engines. Examining the target species set proposed in [69], it is argued that inclusion of certain target species (fuel, HO_2, CO) can overestimate the importance of the target species for certain combustion stages. In particular, during the post ignition stage at high temperatures, almost all of the large hydrocarbons have broken down into small molecules, thus only CO oxidation and H_2-O_2 reactions play an important role, and a more appropriate target set is (HO_2, CO). Further, once the system undergoes complete combustion or reaches near equilibrium, none of the original target species are important anymore as the system has

shifted to CO_2 and H_2O production; an appropriate target set would be (CO_2, H_2O). Thus, dynamic selection of target species based on the local thermochemical state is necessary to achieve maximal efficiency of the DAC scheme. An extended DAC scheme (EDAC) for switching between various target sets based on thresholds of two progress equivalence variables was proposed. It was also found that species inside the NO sub-mechanism were not included except in narrow temperature and equivalence ratio ranges, depending on the NO sub-mechanism used. As this could result in large errors in NO_x predictions, NO was recommended to be added to the target species set if the temperature was over a critical value (e.g. 1800K). It is noted that if NO is present in the mixture (e.g. in exhaust gas recycling simulations) the DAC/DRGEP scheme is capable of accounting for hydrocarbon/NO sensitization effects on the ignition process without including NO in the target species set. Finally, once combustion has completed (as determined by temperature and the progress equivalence variables) the DRGEP cutoff value could be increased by a factor of ten without any loss in accuracy.

It was found that the base DAC scheme was capable of achieving a 30%–50% time savings for two small n-heptane mechanisms, with an extra 8–10% time savings achieved through use of the EDAC scheme. It is noted that the DAC scheme should not be applied to computational cells with liquid fuel droplets so as to avoid any adverse effects on evaporation model predictions. However, in the proposed EDAC scheme, the progress equivalence ratio tolerances for switching between target species sets and DRGEP cutoffs were derived empirically from zero-dimensional studies; thus they may not be applicable for all combustion problems and chemical mechanisms. When combined with an adaptive multi-grid technique [80] a factor of four speedup was found for DI engine simulations. The combination of the DAC scheme and the adaptive multi-gridding technique also enabled a multi-dimensional engine simulation using a detailed chemical mechanism (543 species) to be completed in a practical amount of time. It is noted that the overhead of the EDAC scheme did reach ~5% of total computation time for some cases.

1.6 Goals

This work sought to determine a method of selecting DRGEP target species solely based on the local thermochemical state of the system. As with the EDAC method, this will allow DAC simulations to respond to changing combustion conditions, maintaining accuracy and computational efficiency where a single DRGEP target species would fail. However unlike the EDAC scheme, the proposed method will not be limited to a fixed set of static target species sets, ensuring that accuracy and efficiency will be maintained even for unexpected combustion conditions. The proposed method will also be generally applicable, unlike the EDAC method which was developed for a specific application. Finally, the proposed method will aid the average user in running a DRGEP based DAC simulation, as determining appropriate DRGEP target species will be easier compared to the current methods of target species selection.

1.7 Chapter Outline

In Chapter 2, the goals discussed in Section 1.6 will be expanded upon. In Chapter 3, a methodology for determining appropriate DRGEP target species based solely on the local thermochemical state will be detailed. In Chapter 4, the developed method will be applied to constant volume and single cell HCCI simulations in order to demonstrate its validity and performance. Finally conclusions and suggestions for further work will be discussed in Chapter 5.

1.8 Chapter Figures

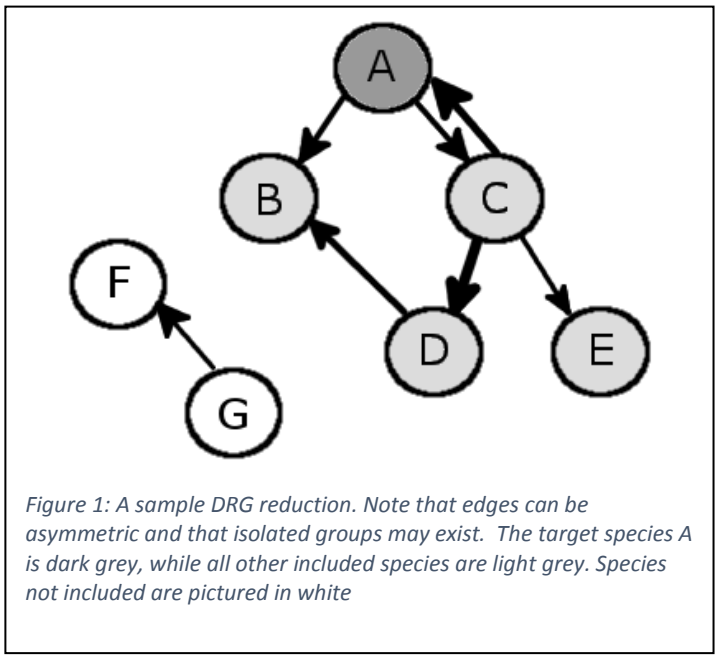

Figure 1: A sample DRG reduction. Note that edges can be asymmetric and that isolated groups may exist. The target species A is dark grey, while all other included species are light grey. Species not included are pictured in white

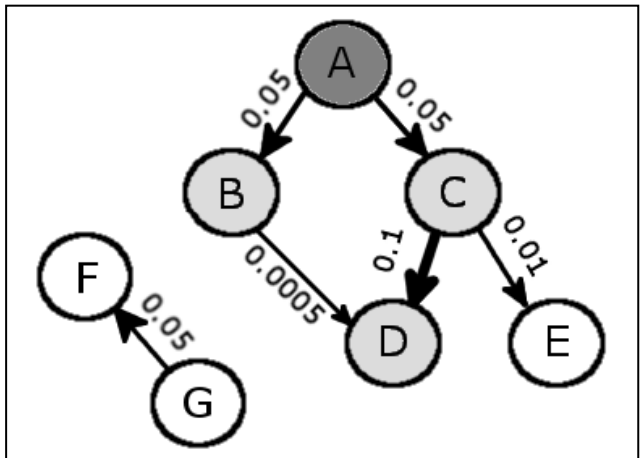

Figure 2: A sample DRGEP reduction with $\varepsilon_{DRGEP} = 0.005$. Note: only forward DICs pictured for clarity. The target species A is dark grey, while all other included species are light grey. Species not included are pictured in white

2. Challenges and Objectives

2.1 Description of Dynamic Adaptive Chemistry Scheme

As the DAC scheme will be used in this section to compare the performance of static target species sets a description of its implementation is presented. All calculations are completed using a version of the open-source chemical kinetics software Cantera [81], modified to allow dynamic mechanism reduction as well as enable dynamic adaptive chemistry integration. The implementation of the DAC scheme follows the form presented by Liang et al. [68], as seen in Eq. 11. The simulation time step is set to $5 * 10^{-6}$s (although the internal integration time step does vary), and the integrator/Jacobian was reinitialized at each simulation time step to account for the changing problem size.

2.2 Static Target Species Selection

Traditionally when using the DRG/DRGEP methods, the user is required to specify a list of target species known to be important to the phenomena of interest. Typical choices of these target species include the fuel, oxygen and combustion products (e.g. CO_2) as well as certain key radicals known to be good indicator species (e.g. H, OH, CO, HO_2) [69, 75, 77]. Other species such as NO_x and other pollutants can be added to the target set if accuracy is required in their prediction. In this context, such a choice of an unchanging set of target species (removal of species from the target set based on mass fraction notwithstanding) is termed a static target species set.

Most attempts to determine appropriate sets of target species performance have consisted of direct comparisons of small numbers of competing static target species sets. However, as Shi et al. [23] demonstrated, the proper choice of target species may vary depending on the local combustion state. Selection of a target species set based on the local thermochemical state will be termed dynamic target species selection.

2.3 Effect of Target Species Selection on the Accuracy and Efficiency of the DRG and DRGEP Methods

N-Heptane is an important primary reference fuel (PRF) for gasoline that has been extensively studied in literature. N-Heptane exhibits strong negative temperature coefficient (NTC) behavior as well as two-stage ignition behaviors in the low temperature chemistry regime [82], and due to its large size its oxidation differs considerably from smaller hydrocarbons like methane and ethylene. These factors require a higher level of fidelity for produced skeletal mechanisms, as large errors can accumulate rapidly. For this reason, Version 2 of the LLNL detailed n-heptane mechanism (561 species) [71, 83, 84] has will be used in this chapter for investigation into the effect of choice of target species.

As discussed in section 1.3.3.2, in the DRGEP method species further away from the target set on the DRGEP graph are more likely to be removed due to the error propagation step. While this *can* result in a smaller skeletal mechanism size for a similar error level when compared to a skeletal mechanism generated using the DRG method, it also implies that the proper selection of target species is more important for the DRGEP method; improper selection of target species can actually make the resultant DRGEP skeletal mechanism larger or considerably less accurate.

In Fig. 3, a single cell HCCI engine simulation using the n-heptane mechanism under the conditions listed in Table 1 is investigated. The top figure shows the resultant temperature trace of this simulation; a two stage ignition process is predicted. The lower graph displays a comparison of performance metrics for the DRG/DRGEP simulations for different target species sets. The mass fraction cutoffs for the DRG/DRGEP target species were set to 10^{-12} and 10^{-30} respectively, in accordance with past recommendations [69, 75]. The DRG/DRGEP cutoff values were set to 0.01 and 0.001 respectively, such that the error in ignition delay was roughly similar between the two methods.

In Fig. 3 it is seen that the accuracy of the DRG based DAC scheme is insensitive to the changing target species sets; the error in ignition delay is nearly constant. As the DRG method does not include

any sort of error propagation, the entire set of species important to n-heptane breakdown is included by choice of n-heptane as a target species. As the OH and HO_2 radicals will be likely important to n-heptane breakdown, they will be included in the local skeletal mechanisms for most of the simulation; as well, all species important to them will be included in the local skeletal mechanism. In essence, before ignition both will act as target species even if not explicitly included in the target species set. A similar phenomenon is expected of CO once carbon dioxide production becomes an important combustion process. The side effect of this phenomenon is that the average number of active species before ignition is roughly constant for all target sets; therefore the accuracy and reduction level of the DRG method for DAC simulations is largely controlled by the DRG cutoff value. On the other hand, the DRGEP based DAC scheme is highly sensitive to the selected target species set.

For the DRGEP based DAC simulations, it is seen that for the target species sets (n-heptane, CO), (n-heptane, CO, HO_2), the error in ignition delay is considerably reduced. However, using simply (n-heptane) as the target species set greatly increases error, while adding OH to the target species set (n-heptane, CO, HO_2) increases the error level to near that of the DRG based DAC simulations. This underscores the importance of selecting DRGEP target species that are applicable to the combustion problem at hand; by adding target species not directly relevant to the problem under consideration the error of the DRGEP based DAC simulation can actually be increased.

Before ignition (except in the case of the full target species set) the average number of species evaluated for the DRGEP based simulations is ~10 less than that of the DRG based simulations. Further, post ignition the DRGEP based simulations evaluate ~12–15 species on average, a significant improvement over the DRG based simulations which evaluate ~30 species on average. However, when OH is added to the DRGEP target species set both methods have produce similarly sized local skeletal mechanisms. It is noted that for the target species containing solely n-heptane, the target species set becomes empty after ignition as the mass fraction of n-heptane becomes less than the mass fraction cutoff

for both cases. As a result, the DRG/DRGEP simulations tend to turn off chemistry evaluations post ignition; hence the post-ignition average of active species is ~0 for both cases.

Fig. 3 demonstrates that with proper choices of target species, the DRGEP method can be more accurate with smaller local skeletal mechanisms, implying a greater potential speedup. In the DAC scheme, the goal is to quickly produce the smallest local skeletal mechanism that can accurately model the combustion process at that local thermochemical state; maintaining accuracy while achieving the maximum possible speedup. For this reason, the DRGEP method has been selected as the method of choice for this study.

2.4 Range of Applicability for Static DRGEP Target Species Sets

As seen in Section 2.3, the choice of target species can have a large effect on both the accuracy and computational efficiency of the DRGEP method. However, as demonstrated in this section, it is not always simple to choose a single static target species set that is appropriate for all combustion processes.

Consider Fig. 4 in which the DRGEP based DAC scheme is applied to constant volume ignition simulations of n-heptane at 5 and 20 atm at equivalence ratios of 0.5, 1, and 2. The most accurate target species set from Fig. 3 (n-heptane, HO_2, CO) is compared to the target species set (n-heptane, HO_2, CO, OH). The mass fraction cutoff for target species inclusion in the target set is again set to 10^{-30}. The DRGEP cutoff value was set to 10^{-4}, which had been found in [68] to provide a good balance between accuracy and computational efficiency.

It is seen in Fig. 4 that the static target species without OH is considerably less accurate in the transition between the NTC and high temperature chemistry regions of the ignition delay curve; the maximum error increases from 12% to 22% in the 20 atm. autoignition delays and 5% to 16% in the 5 atm. autoignition delays without OH in the target species set. It might be concluded that OH should be included in the target species set for the most generally applicable target species set for n-heptane, however as seen in Fig. 3 the inclusion of OH into the target species set considerably increased the error

in ignition delay predictions for a single cell HCCI simulation, while simultaneously increasing the resultant skeletal mechanism sizes. This leads to the conclusion that a single static target species set may not be optimal for all combustion conditions; in line with the work of Shi et al. [23]. Although this is not an issue in relatively simple combustion problems where the major combustion conditions can be known apriori with reasonable certainty, it may become an issue in large multi-dimensional simulations where the expected combustion conditions are more uncertain (see Section 1.4). If unexpected combustion conditions are encountered in a large multi-dimensional simulations, a target species in a static DRGEP target species set may become unimportant or irrelevant, and the computational efficiency or accuracy of a DRGEP based DAC scheme may be impacted.

2.5 Development of a Dynamic Target Species Selection Strategy

In order to ensure that accuracy and efficiency are maintained, a dynamic target species selection strategy is needed for DRGEP based DAC simulations. The EDAC scheme proposed by Shi et al. [23] depended on empirically determined constants to switch between different static target species sets, however it is not necessarily straightforward to adapt this approach to other problems and chemical mechanisms. Instead this work will focus on selecting appropriate DRGEP target species based solely on the local thermochemical state. By doing so, the following will be achieved:

1. Like the EDAC method, this dynamic target selection method will be able to respond to changing combustion conditions. However, unlike the EDAC method, the proposed method will not be limited to a fixed set of static target species sets, ensuring that accuracy and efficiency will be maintained even for unanticipated combustion conditions.
2. The method will be generally applicable, whereas the EDAC method was developed with a specific application in mind, potentially posing a challenge to when reconfiguring for different problems and chemical mechanisms.

3. As appropriate target species will be determined from the local thermochemical state, this method should require little user knowledge to determine DRGEP target species as compared to static target species selection.

2.6 Chapter Figures and Tables

Table 1: N-Heptane engine simulation conditions. Engine properties from [85], initial modified from [74]. Simulation begins at Crank Angle = 99°	
T_0 (K)	421
P_0 (bar)	3.2
RPM	900
φ	0.5
Connecting Rod / Crank ratio	3.2
Displacement Volume (L)	0.981
Compression Ratio	14

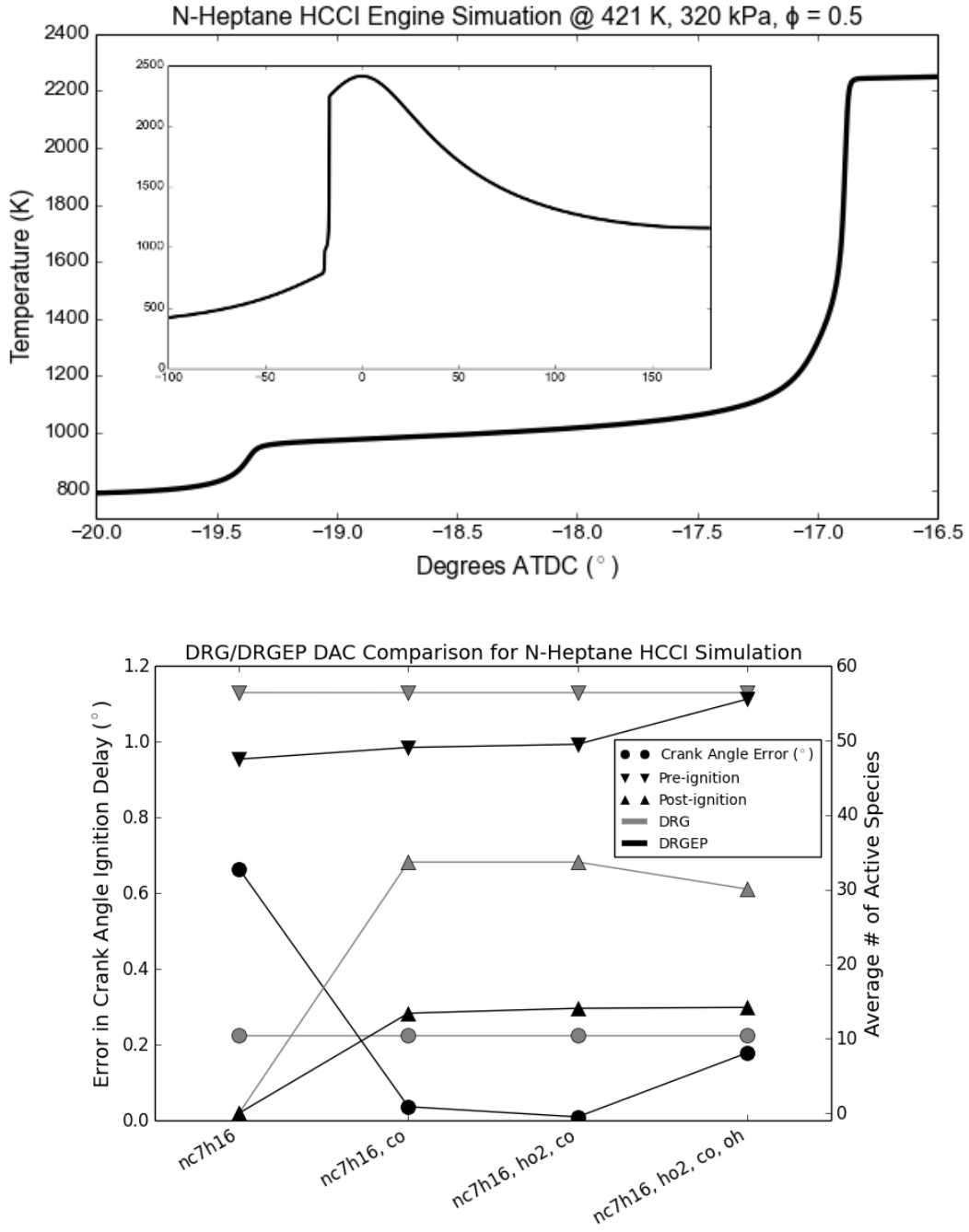

Figure 3: Top: temperature trace of HCCI simulation for full n-heptane mechanism under initial conditions listed in Table 1. Bottom: Comparison of error and resultant mechanism size of target species sets for DRG/DRGEP DAC simulation of single cell n-heptane HCCI simulation. Minimum target species mass fractions were set to 10^{-12} and 10^{-30} for the DRG/DRGEP simulations respectively, in accordance with [71] and [65]. DRG/DRGEP cutoff values were set to 0.01 and 0.001 respectively, such that the error for the full target set was similar between methods.

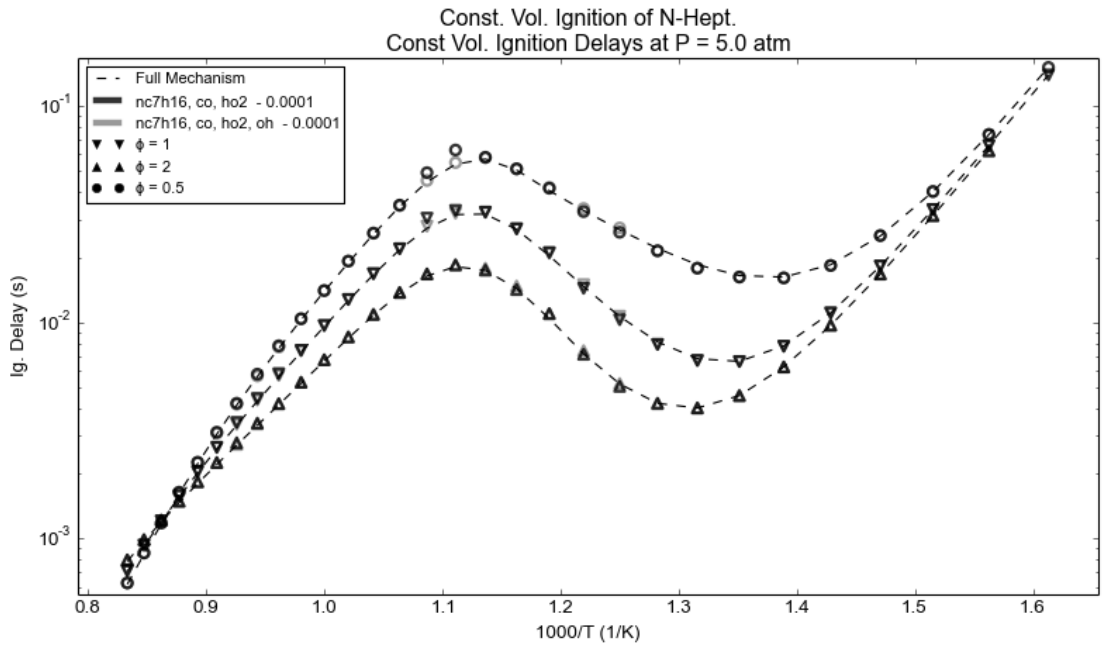

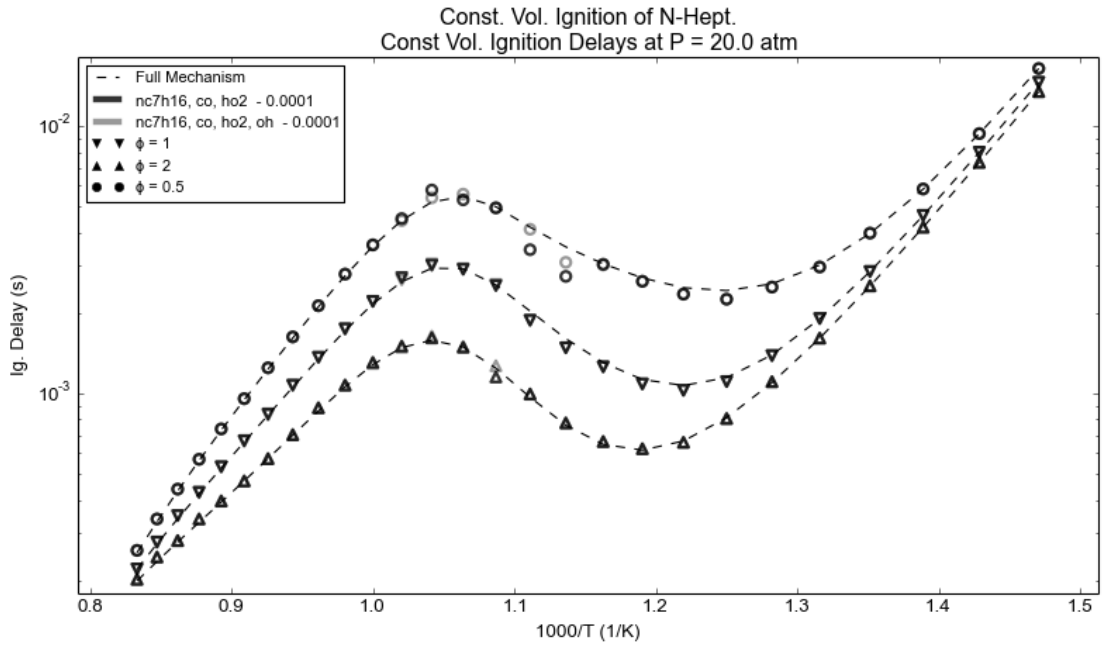

Figure 4: Comparison of two static target species sets for constant volume n-heptane ignition delays. By adding OH to the target species set the maximum error decreases from 22% to 12% for the 20 atm cases, and 16% to 5% for the 5 atm cases. The DRGEP cutoff value was set to 10^{-4} for both cases and the minimum mass fraction for a target species to be included in the target species set was set to 10^{-30} in accordance with [65]

3. Dynamic Target Species Selection

3.1 Sample Ignition Studies

To develop this method of dynamic target species selection n-heptane constant volume ignition studies will be examined using Version 2 of the LLNL detailed n-heptane mechanism (561 species) [71, 83, 84]. In order to investigate the effect of differing combustion pathways, two sample cases will be taken from the high and low temperature regimes of n-heptane constant volume autoignition at an initial pressure of 2 atm (Fig. 5). The first case (700 K, 2 atm, $\phi = 1$) lies in the transition from the NTC chemistry regime to the low temperature chemistry regime. It exhibits a two stage ignition process; after first stage ignition most of the n-heptane has been exhausted and the temperature is ~900K (Fig 6). The second case (1000K, 2 atm, $\phi = 1$) lies in the transition from the NTC chemistry regime to the high temperature chemistry regime, and exhibits a single stage ignition process (Fig 6). By selecting ignition studies in ranges where different chemical processes dominate, the effect of chemistry on the proposed method can be investigated. Additionally as the temperature of the 700K case after first stage ignition is similar to that of the 1000K case, an opportunity is provided to investigate the effect of temperature on changing chemical pathways.

3.2 Examination of the Directed Relation Graph with Error Propagation Structure

To understand this method of determining target species the meaning of the DRGEP coefficients must first be examined (Fig. 7). The DRGEP adjacency matrix (Fig. 7) in this study is formatted in row-major format; the value at row *i*, column *j* is the DRGEP direct interaction coefficient representing species *i*'s dependence on species *j* (i.e. r_{ij}). If r_{AB} is large, species *B* is considered important to the production or consumption of species *A*; similarly, if r_{BA} is large, species *A* is considered to be important to the production or consumption of species *B*. Summing all DRGEP coefficients in column *A* (Fig. 7):

$$Column\ Sum(A) = \sum_{B_i \in neighbors(A)} r_{B_i A} \tag{12}$$

A species with a large column sum will be important to the production/consumption of many other species, and therefore will be very active in the mechanism. However, since the column sum of a species is dependent on the number of neighbors it has in the mechanism, it cannot be used directly to make comparisons between different species. Yet, a sense of its utility in tracking the activity of a species can be observed by comparing column sums of the same species in different ignition cases, as demonstrated in Fig. 8.

In the 700K ignition case, much of the n-heptane is consumed during first stage ignition; as a result the column sum of n-heptane drops off significantly. The column sum of CO_2 remains small throughout the process, indicating that it reacts with relatively few species. In the low temperature region before first stage ignition, the column sum of O_2 and OH are particularly large as a result of the enhanced R-OH and R-O_2 chemistry. Additionally the column sums of HCO and HO_2 are much lower in this region, indicating they are less important to the mechanism at this lower temperature state. After first stage ignition, the column sums of all species except n-heptane reach levels similar to that of the 1000K case, indicative of the temperature effect of the changing strength of chemical pathways.

The absence of a multiple stage ignition event in the 1000K ignition case manifests in far more gradual changes in the column sums. The column sum of n-heptane steadily declines as it is consumed. The column sum of the HCO radical steadily increases throughout the induction period, as it becomes more important to CO_2 production. The column sum of OH stays roughly constant throughout ignition, while the column sum of HO_2 declines approaching ignition as its primary consumption pathway, via n-heptane reactions, slows down. Finally, CO_2 has a small column sum throughout the process, similar to the 700K case.

3.3 Target Species Roles

Common choices of target species tend to fall into one of two categories, important radicals (e.g. OH, HO_2…) and important reactants and products (e.g. n-heptane, O_2, CO_2, CO…). In Fig. 9, a sample

local DRGEP reduction of the n-heptane mechanism [83] using either n-heptane or the OH radical as a target species is examined.

Examining the immediate neighbors of n-heptane on the DRGEP graph, it becomes clear that n-heptane only directly includes a few species, but tends to be strongly dependent on each. Most species included in the resultant skeletal mechanism are kept due to their importance to the first ring of strongly linked species. This type of target species behavior will be designated a 'locally important' target species due to its strong, but localized link to a few species. It has been found that CO, CO_2 and n-heptane tend to behave as locally important target species.

Examining the OH reduction graph reveals a different pattern. Most of the species included are one step away from OH on the graph, and are weakly linked to it. As a result, relatively few species more than one step away are included. Further, those included species farther away from the first ring of weakly linked species tend to be very strongly linked to a species in that ring. This type of target species behavior will be designated a 'globally important' target species, due to its direct, but weak, link to so many species. It has been found that most radicals, e.g. OH, HO_2, behave as globally important target species. Additionally, non-radicals involved in many reactions, e.g. O_2 behave as globally important target species. The number of reactions and neighboring species for each of the commonly used target species is listed in Table 2.

In the case of oxygen, there are many potential reactions with a large number of species; however, except for the case of low temperature chemistry relatively few of these pathways are strongly reacting. This leads to the lower column sum values of oxygen compared to OH and HO_2 as seen in Fig. 8. In general, global target species will tend to have larger column sums as they react with many more species than locally important target species, making the column sum alone insufficient to compare species as potential target species.

3.4 Column Sum Normalization

As the magnitude of the column sum of a species is roughly dependent on the number of neighbors it reacts with, it is natural to look for a normalizing factor that will be tend to be smaller for species with many active neighbors. In the n-heptane mechanism used the OH radical is involved in 1051 reactions with 519 different species, while n-heptane is only involved in 140 reactions with 36 species. As OH radical reacts with so many species, any neighboring species will only be involved in a relatively small percentage of its reactions. However, n-heptane reacts with relatively few species, leaving the possibility open that a single species will be involved with most of its production or consumption. From Eq. 4, it can be inferred that the average DRGEP coefficient from OH to its neighbors:

$$\overline{r_{OH}} = \frac{\sum_{B_i \in neighbors(A)} r_{AB_i}}{\sum_{B_i \in neighbors(A)} \delta_{AB_i}} \tag{13}$$

where:

$$\delta_{AB_i} = \begin{cases} 1 \; r_{AB_i} > 0 \\ 0 \; r_{AB_i} = 0 \end{cases} \tag{14}$$

will be much smaller than the average DRGEP coefficient from n-heptane to its neighbors. That is:

$$\overline{r_{OH}} \ll \overline{r_{nc7h16}} \tag{15}$$

Consequently, Row Average of a species *A* is defined as:

$$Row\ Average(A) = \frac{\sum_{B_i \in neighbors(A)} r_{AB_i}}{\sum_{B_i \in neighbors(A)} \delta_{AB_i}} \tag{16}$$

This definition gives the average of the active entries in row A of the DRGEP adjacency matrix; a globally important target species will have many active neighbors, but will tend to be weakly dependent on all but a few, resulting in a lower row average. A locally important target species will have few active neighbors but will tend to be more strongly dependent on each, resulting in a higher row average.

Plotting the row average (Fig. 10) for some commonly used target species, it is seen that the relation predicted in Eq. 15 holds; in both ignition cases the row average of OH is almost an order of

magnitude smaller than that of n-heptane. Further, the species expected to be locally important targets (e.g. HCO, n-heptane and CO_2), as listed in Table 2, have row averages at least an order of magnitude larger than the globally important target species (e.g. O_2, OH, HO_2) in both ignition cases.

3.5 Definition of the Relative Importance Index

Using the row average as a normalizing factor; we define the relative importance index (RII) as:

$$RII(A) = Row\ Average(A) * Column\ Sum(A) \quad (17)$$

The RII of a species attempts to balance the column sum and row average of a species, allowing both globally and locally important target species to be selected.

In Fig. 11, we examine the RII values of commonly used target species throughout the sample integration cases. In both cases the RII of OH remains one of the largest values throughout the integration. Further, the RII of OH and O_2 are significantly higher in the low temperature chemistry region. In the 700 K ignition case the RII of n-heptane begins to decline as it is consumed during first stage ignition, while the RII of HCO and HO_2 rise as new pathways open leading up to the ignition event. Finally, the RII of CO_2 remains relatively low throughout the process, increasing slightly during first stage ignition and before the final ignition event.

Initially in the 1000K case, the RII of HO_2 and n-heptane track with each other, as HO_2 consumption is strongly coupled to n-heptane reactions; closer to ignition this phenomena stops as HO_2 switches to ethyl and carbon monoxide reactions. Near the beginning of the simulation, OH consumption and production is strongly tied to a few species (e.g. n-heptane reaction forming heptyl radicals) but as the induction period progresses, OH consumption and production become weakly tied to reactions with many species; as a result the RII of OH drops throughout. The RII of HCO continues to increase throughout the simulation, as HCO → CO → CO_2 becomes a more important pathway for CO_2 production. Finally, carbon dioxide has a small RII throughout the simulation, but starts to increase right before ignition, similar to the 700K case.

It is interesting to note that outside of the low-temperature chemistry zone, oxygen has a relatively RII value due to its low column sum and row average. This implies that other species in the mechanism depend relatively weakly on oxygen and that oxygen consumption is only weakly dependent on any single species. However, without oxygen (or another oxidizer) there would be no combustion reaction at all. This leads to the conclusion that the RII value of a DRGEP target species is more closely related to the local importance of a species on the directed relation graph, rather than its overall importance to the mechanism.

3.6 Target Selection Process

From the DRGEP coefficients computed during reduction, the RII of each species can be calculated. Moreover, it is trivial to add the calculation of active neighbors, column, and row sums to the pre-existing DRGEP calculation loop, meaning that this method can be executed with negligible overhead. Only a single extra loop that scales proportionally to the number of species in the mechanism is needed to put this information together to calculate the RII value. In this loop, each species mass fraction is tested; if it is greater than a minimum threshold, the species is inserted into a priority queue with priority equal to its RII value. If the queue size is larger than the total number of RII targets to be selected, the species with the minimum RII value is popped off the queue. Depending on the priority queue implementation, the cost of each insertion/removal pair from the priority queue scales linearly or logarithmically with the maximum size of the queue (the number of RII target species to be selected). However, since the number of RII target species is a small fixed number, the overall cost can be considered constant time in asymptotic analysis, i.e., O(1). Therefore the total additional overhead of this method compared to using a static target species set scales linearly with the number of species in the mechanism.

Consider a potential target species *A* that only participates in a single reaction. Species *A* will have a row sum of unity by definition; all of its consumption and production must depend on the only

species that it reacts with. If these neighboring species also participate in relatively few reactions (a definite possibility) then the DRGEP coefficients:

$$r_{B_i A} \; for \; B_i \in neighbors(A)$$

will tend to be closer in value to one, as each neighbor B_i will react with only a handful of species. As a result the column sum of *A* will be roughly equal to the number of neighbors, meaning that the RII value of species *A* will be larger than expected for such a species. To avoid such an over inflation in the RII value of species *A*, it is recognized that such a species is likely to exist in small quantities during combustion, as it will tend to be a single step in a long reaction pathway. In order to counter act this potential biasing of RII values, only species with a mass fraction greater than a small threshold (e.g. $Y \geq 10^{-10}$) are considered during the target selection process.

In Fig. 12, the targets selected most often throughout the 700 K ignition case are examined. In the first stage ignition n-heptane and O_2 are initially chosen as a target species. O_2 is selected due to the minimum mass fraction requirement, as well as the enhanced R-O_2 chemistry in this region. Shortly thereafter, two seven carbon ketones (NC_7KET_{35} & NC_7KET_{42}) are selected as target species. These ketones play a large role in the creation of OH, via both their creation and decomposition, and lay along major pathways in the low temperature breakdown of n-heptane. At approximately 0.004s, c2h5coch2, a major product of the decomposition of these ketones begins to be selected as a target species. Additionally, c2h5coch2 lies along an important path for early CO_2 production. Once appropriate OH levels build up, OH is continually selected for the rest of the simulation. As OH is known to be important even in small concentrations for these low temperature, first stage ignition processes, it has been found to be beneficial to relax the OH mass fraction cutoff (e.g., $Y_{OH} \geq 10^{-15}$) in order to maintain accuracy in this combustion regime. This procedure was also extended to other specific key radicals (e.g., HO_2) in order to promote their earlier selection as target species.

After first stage ignition HCO is initially selected as a target species, once the HCO created during first stage begins to react. Once the HCO level is depleted, it is no longer selected as a target

species. Shortly thereafter, formaldehyde (CH_2O), another important CO_2 precursor, begins to be selected as a target species. It will be continually selected until final ignition, when HCO becomes an important CO_2 producer again. Finally we see that CH_2CHO, another strong CO_2 producer via a reaction forming HCCO, is selected as a target species throughout second stage ignition. In the post-ignition stage, only species involved in the H_2-O_2 and CO oxidation reactions are selected as targets. In this case, this means the selection of H_2O_2, HCO, and HO_2.

In Fig. 13, the target selection of the 1000 K ignition case is examined. N-heptane is again initially selected, but in this simulation the higher temperature creates OH and HO_2 fast enough such that they are selected almost from the beginning of the simulation. At these initial conditions, n-heptane destruction via HO_2 reactions is favored, as well as OH creation via HO_2-methyl/ethyl reactions. As a result, HO_2 remains important for much of the early simulation. Relatively early in the simulation CH_2CHO begins to be selected. Although it is not particularly important to the production of CH_2O and CO, nearly 100% of the CH_2CHO formed decays into these species, providing an excellent path into the other strongly reacting CO_2 pathways. Later, C_3H_5-t is selected as a target species. C_3H_5-t is strongly coupled to propylene (C_3H_6) and CH_3COCH_2, and lies on a major pathway connecting heptyl radicals to CH_2CO and other CO_2 producing pathways in this region. Finally just before ignition, HCO begins to be selected as a target species again as the HCO → CO → CO_2 pathway becomes important to CO_2 production. Post-ignition, the same set of species (H_2O_2, HCO, and HO_2) covering H_2-O_2 and CO oxidation reactions are selected.

3.7 Chapter Figures

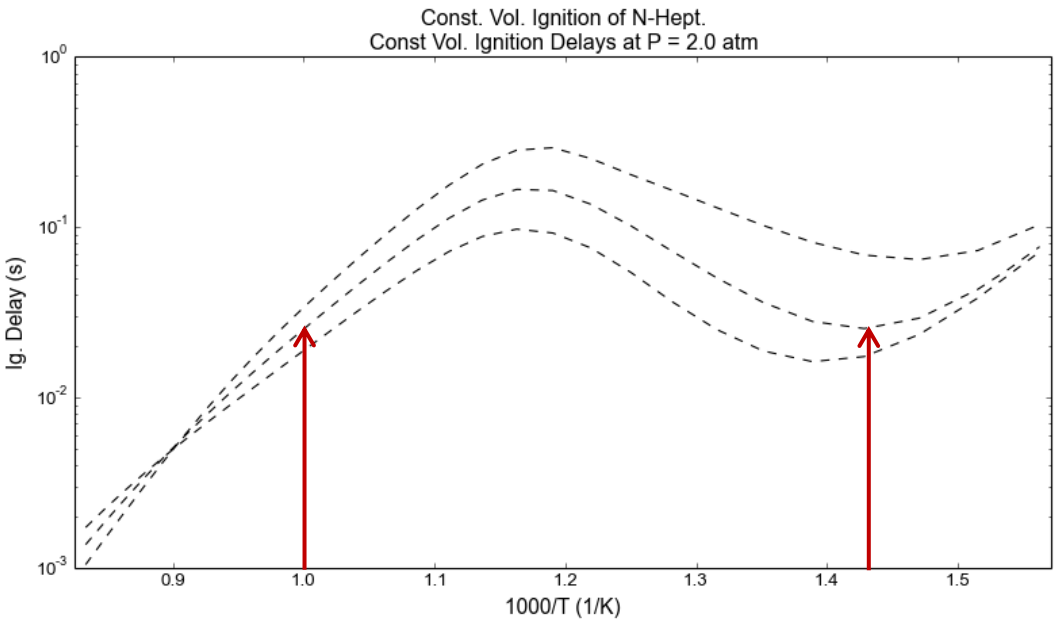

Figure 5: Ignition delay curve of constant volume n-heptane ignition at two atmospheres and equivalence ratio equal to one. The selected sample cases are marked with arrows

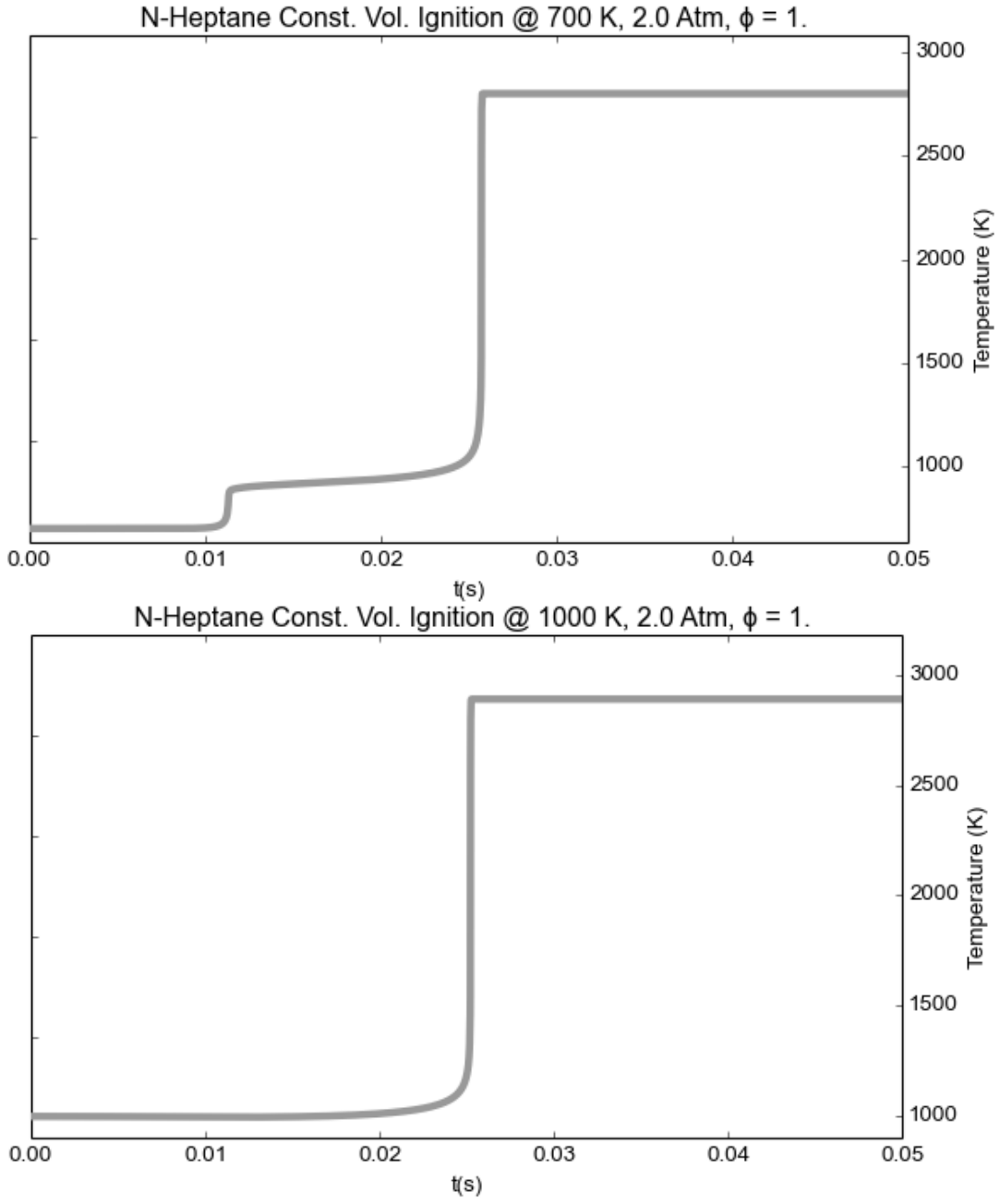

Figure 6: Temperature traces of the two selected constant volume n-heptane ignition cases, 700K (top) and 1000K (bottom) at 2 atm and equivalence ratio equal to one.

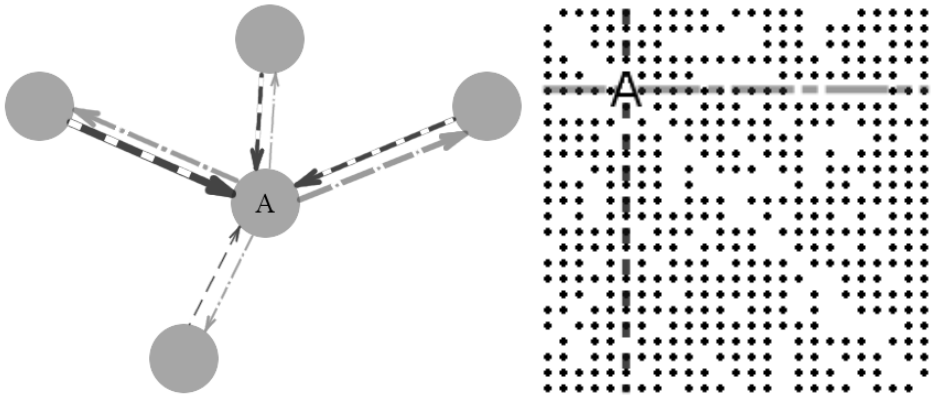

Figure 7: A representation of a graph created from DRGEP coefficients, and their corresponding structure in the adjacency matrix. Note that a true adjacency matrix would be symmetric

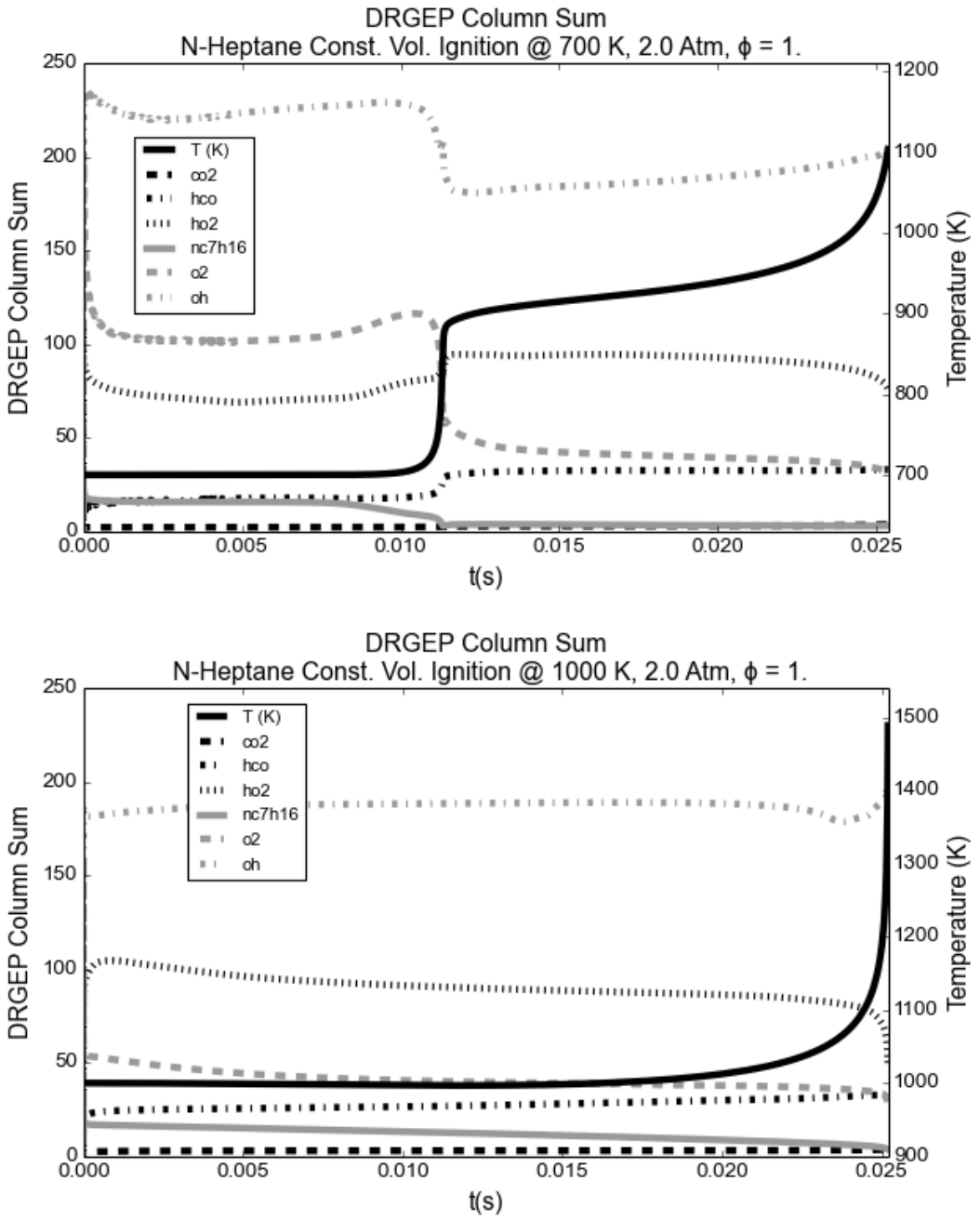

Figure 8: DRGEP column sum during constant volume n-heptane ignition for the two constant volume ignition cases show in Fig. 6

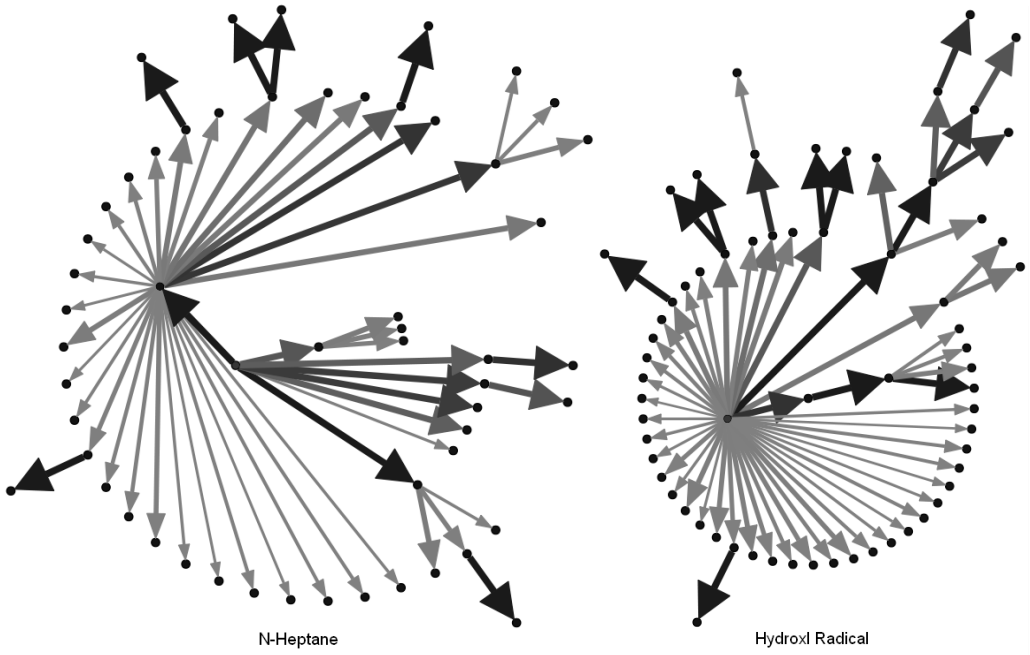

Figure 9: A sample DRGEP reduction with $\varepsilon_{DRGEP} = 10^{-5}$ for two choices of target species. N-Heptane is strongly linked to a few species, while the Hydroxyl radical is weakly linked to many species. Arrow size and color indicate magnitude of DRGEP coefficient. Target species are nodes with no incoming edges

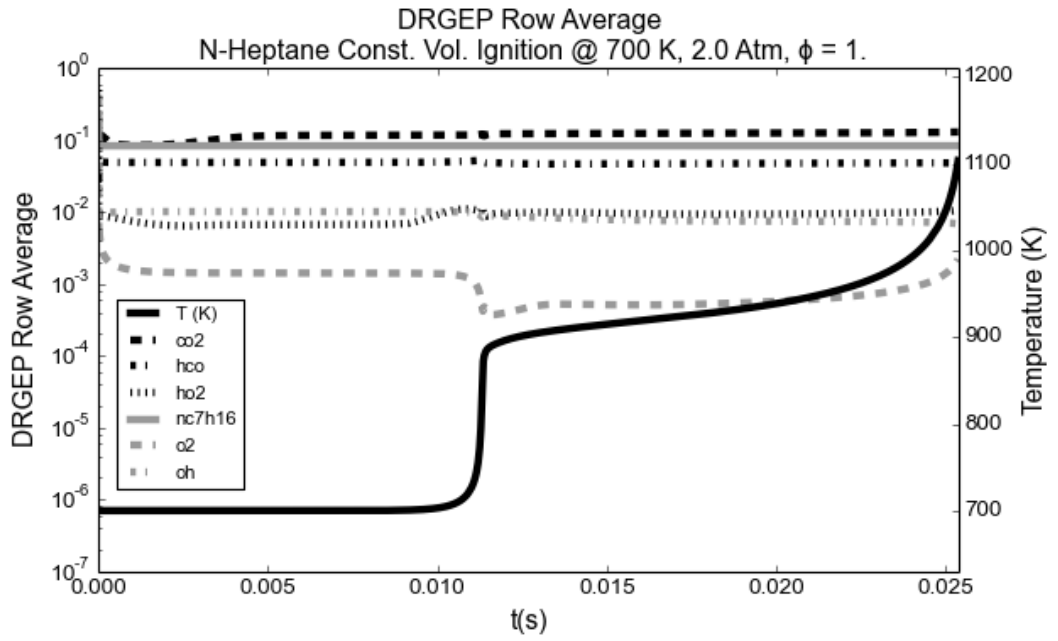

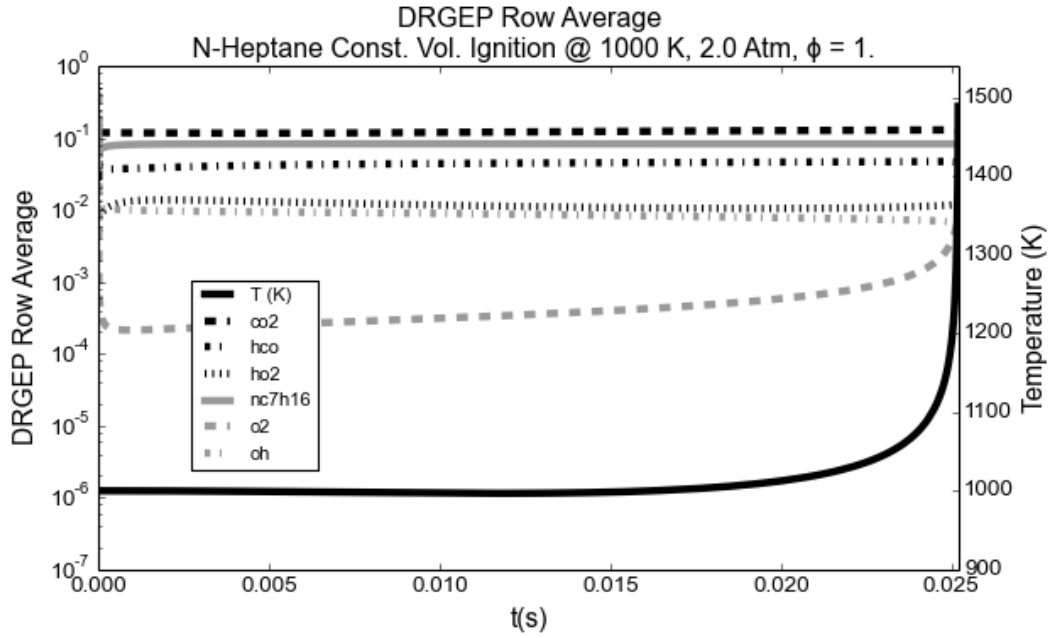

Figure 10: The DRGEP Row Average of commonly selected target species for the two constant volume ignition cases show in Fig. 6

Table 2: Number of neighboring species and reactions for commonly selected target species in the n-heptane mechanism[84]

Species	Number of Neighboring Species	Number of Reactions	Target Species Type
CO_2	25	31	Locally Important
HCO	106	145	Locally Important
HO_2	337	763	Global Important
n-heptane	36	146	Locally Important
O_2	352	624	Global Important
OH	519	1051	Global Important

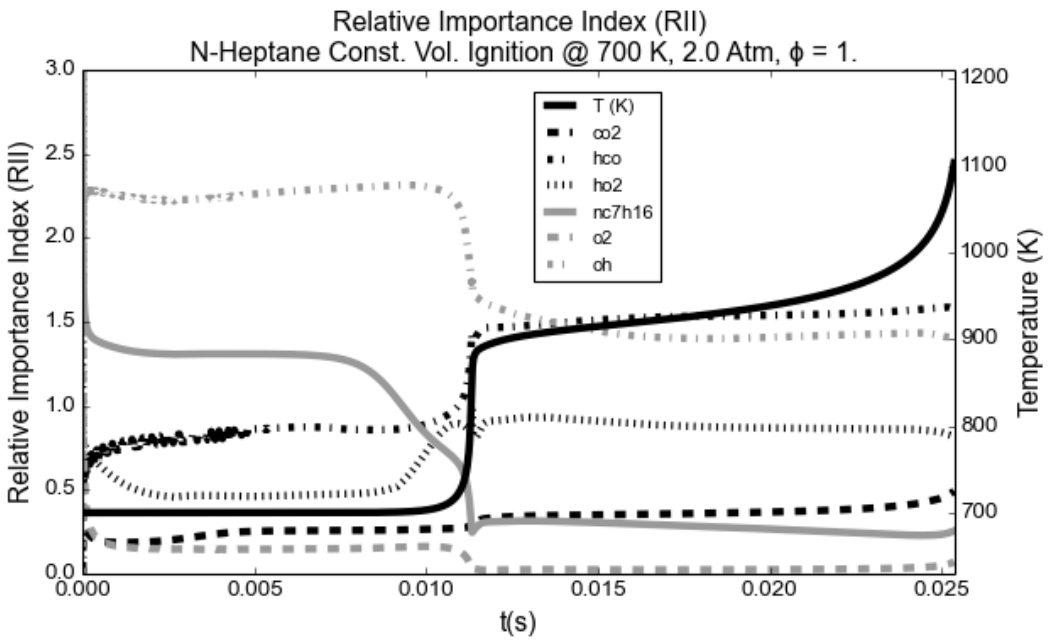

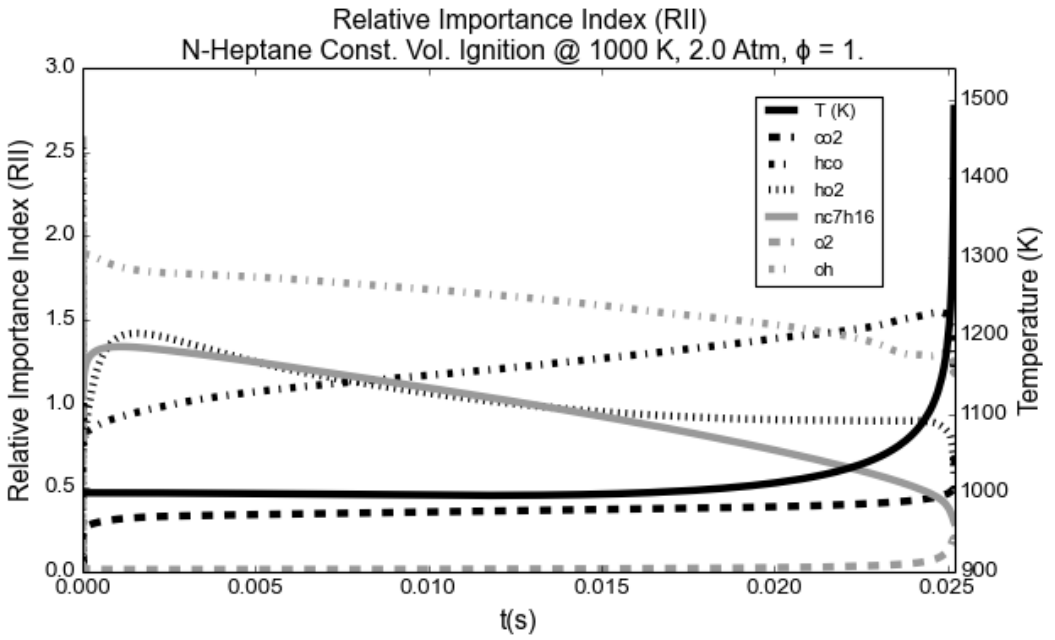

Figure 11: The Relative Importance Index of commonly selected static target species for two sample constant volume ignitions as Fig. 6.

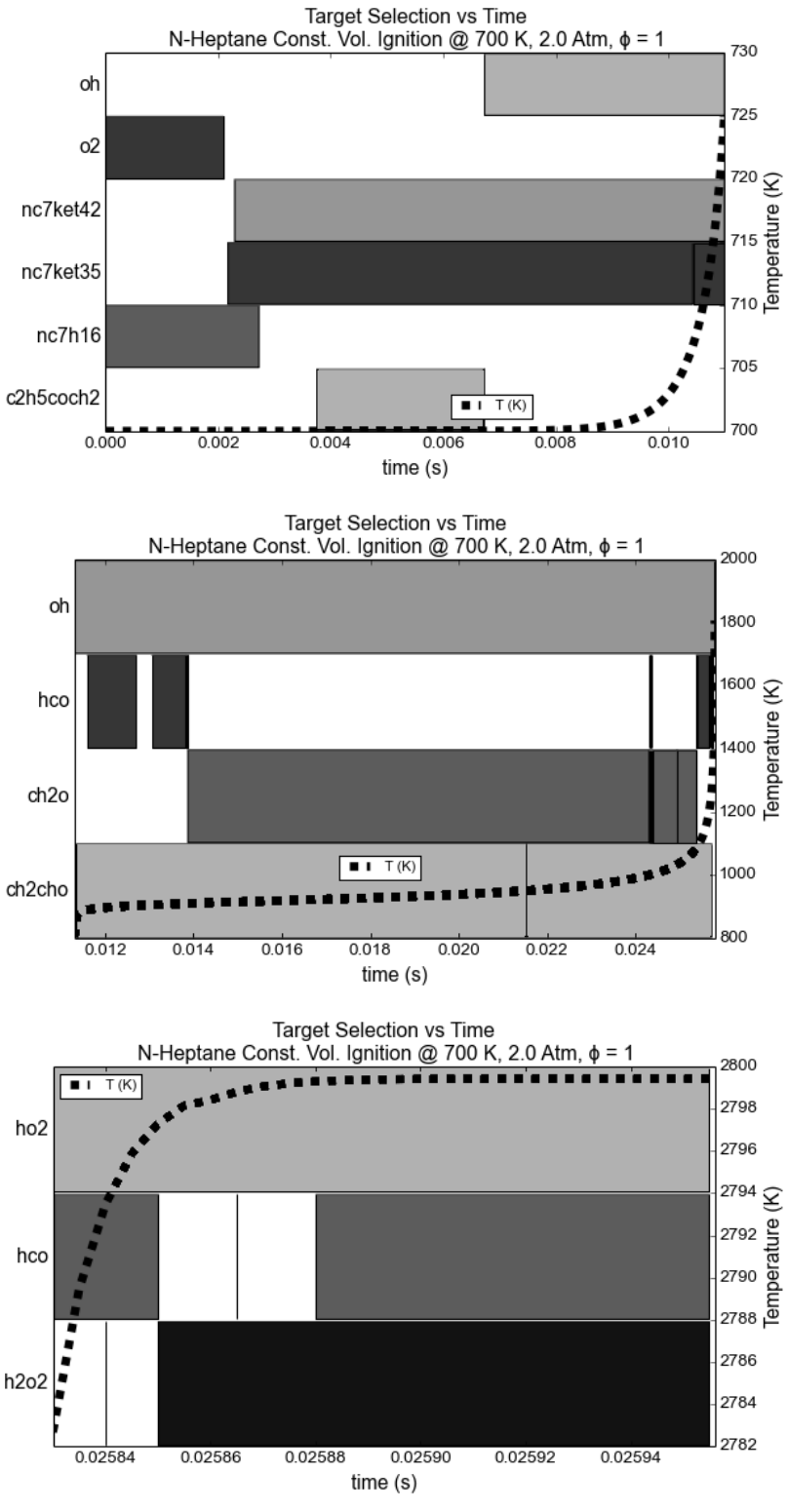

Figure 12: Targets selected by RII method throughout the 700 K ignition case. Species with the top three RII values and mass fraction greater than 10^{-10} were selected to be targets.

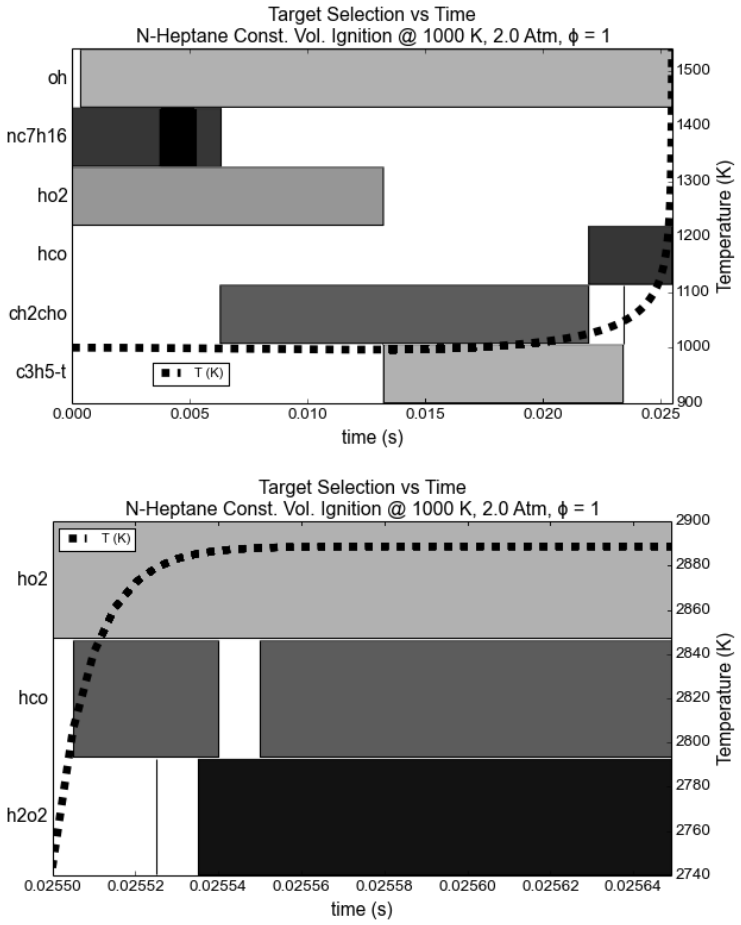

Figure 13: Targets selected by RII method throughout the 1000 K ignition case. Species with the top three RII values and mass fraction greater than 10^{-10} were selected to be targets. The black strip in the n-heptane selection during the induction period indicates that it is rapidly switching between being selected and not selected as a target species.

4. Results

4.1 Simulation Methods

All simulations were performed using the DAC procedure outlined in section 2.1. For constant volume ignition timing runs, the simulation was run until ignition, which was determined as the first time step where temperature was more than 400K greater than the initial temperature. Single cell engine simulations were run taking constant time steps. The crank angle was calculated at each time step, from which the volume of the cylinder could be calculated using the listed engine parameters. The single cell engine simulations were run from a specified starting crank angle until the piston reached bottom dead center (BDC). Simulation wall clock times reported were taken as the average over five runs.

4.2 N-Heptane Engine Simulation

First in Fig. 14 we will reexamine the HCCI ignition case originally presented in Fig. 3 in order to determine the effect of dynamic choice of target species. It is observed that the RII target species behave in a more predictable manner; adding more target species to the RII set results in continuing decline in ignition delay error predictions while the static target species sets exhibit the highly non-linear behavior with growing size as seen in Fig 3.

The top graph in Fig. 14 compares the RII target sets using a DRGEP cutoff of $5 * 10^{-3}$ to the static target species sets using a DRGEP cutoff of 10^{-3}. These DRGEP cutoff values were selected such that the static and RII target species sets have ignition delay error of very similar magnitude. For the most accurate target species sets for both selection methods (five RII species and n-heptane, CO, HO_2 respectively), the RII target set evaluates ~20 less species on average before ignition, and ~5 less species on average after ignition. The bottom graph in Fig 14 compares the RII target sets and static targets species sets both using a DRGEP cutoff of $5 * 10^{-3}$. Although the average mechanism sizes are very close for this case, it is seen that the RII target species sets become considerably more accurate than the static

targets sets as more RII species are added. The RII target sets clearly outperform the static target species sets for this single cell HCCI engine simulation. Further, the RII method is relatively insensitive to the number of RII targets; continually adding RII targets will greatly reduce error when there are only a few RII target species (e.g. one or two), however once there are several RII target species (e.g. three or four), adding more RII target species only marginally decreases the error in ignition delay, while marginally increasing the average species evaluated before ignition.

In general it has been found that the DRGEP cutoff value for a RII target species set should be set to ~2–5 times that of a comparably sized static target species set in order to achieve similar accuracies. In addition, the roughly constant level of accuracy of the RII target species sets with larger numbers of RII species raises some interesting possibilities. For instance, since it is very simple to add relevant target species using the RII method, a 'scattershot' approach—where many RII targets (e.g., 10) are paired with a relatively high DRGEP cutoff value—becomes a viable option. This will be investigated further in the following section.

4.3 N-Heptane Constant Volume Simulations

Next the performance of the RII method on constant volume simulations of n-heptane will be assessed. Sets of static and RII target species are compared; the DRGEP cutoff values were determined by trial and error such that the static and RII target species sets had a similar maximum error in ignition delay. The static target set consisted of n-heptane, HO_2, CO, and OH; the static targets were only included in the target set if their mass fraction was greater than 10^{-30}. The RII target sets consisted of the species with the maximum RII values and a mass fraction greater than 10^{-8} (unless otherwise noted). In all RII cases the mass fraction cutoff was lowered for HO_2 and OH to 10^{-15}.

As the constant volume simulations do not have a fixed end time, but instead were run until ignition, the wall time is not necessarily the best measure of the performance of a target species set. Consider two target species sets that over and under predict ignition delay by 5%. For the longest ignition

delays under consideration, this could be up to the order of 10^{-3} s, or 200 simulation time steps, meaning that the over predicted ignition delay simulation could take ~400 time steps longer than the under predicted case. To account for this potential discrepancy, the simulation wall time is normalized by the ratio of the ignition delay predicted by the DAC scheme to the ignition delay as predicted by the detailed mechanism.

Fig. 15 shows that three RII species set is capable of accurately predicting the ignition delays over a wide range of initial temperatures and equivalence ratios for the n-heptane mechanism at 5 atmospheres. The normalized wall times plot shows a large speedup for the RII method in the high temperature chemistry region, but the static target species set (n-heptane, CO, HO_2, OH) has faster normalized wall times in the NTC region. As the initial temperature is lowered and the curve begins the exit the NTC region, the wall times of both methods become roughly equivalent. Fig. 16 shows the same two target species sets for 20 atm ignition delays; again the RII method is capable of accurately predicting ignition delays for a wide range of initial conditions. The normalized wall times of the RII method for the 20 atm cases follow a similar trend to that of the 5 atm cases; considerable speedup is seen in the high temperature chemistry region, while the RII method tends to be slower in the NTC region. Additionally, an interesting trend of greatly reduced normalized wall times for the RII method is seen further into the low temperature chemistry region of the ignition delay curve for the 20 atm cases. The relevant ignition delay error statistics for the target species sets in Figs. 15 & 16 are summarized in Table 3.

In Fig. 17 and 18, RII and static target species selections with a higher ignition delay error limit (i.e. less than 15%) are explored for the n-heptane mechanism. Two RII targets sets, one with 10 RII target species, mass fraction cutoff of 10^{-10} and a DRGEP cutoff of $5 * 10^{-4}$, and the other with 5 RII target species, mass fraction cutoff of 10^{-8} and a DRGEP cutoff of $2.5 * 10^{-4}$ were able to predict ignition delays with a similar maximum error level compared to the static target species set (n-heptane, CO, HO_2, OH) with DRGEP cutoff of 10^{-4}. The relevant ignition delay errors are summarized in Table 4.

The five RII target species set had faster normalized wall times in the high temperature and low temperature regions for both pressures compared to the static target set; however, in the NTC region, the normalized wall time was typically comparable or worse than the static target species set. The ten RII target species set exhibited considerably faster normalized wall times compared to the static targets set in almost all cases for the 20 atm constant volume autoignition curve. Further into low temperature region, the normalized wall times reach comparable levels to the static targets species set. In the 5 atm autoignition cases, the ten RII target set exhibits the best performance of the three targets sets for all initial conditions except in the transition from the NTC region to the low temperature chemistry region, where slower normalized wall times (similar to those of the five RII target set) are observed.

The ten RII species set in Fig. 17 & 18 is an example of the 'scattershot' approach described in section 4.2. By coupling larger numbers of RII species with a higher DRGEP cutoff value, more of the graph is explored, however species less important to the RII target species are aggressively removed. As a result, the 'scattershot' approach is capable of matching the accuracy of a static target species set, but it has faster normalized wall times for most initial conditions tested. One issue noted is that initially in homogenous combustion problems relatively few species have mass fractions greater than 10^{-8}; if only five species have an appropriate mass fraction then the RII method will not select a full ten target species, instead only five targets will be selected. However, using the higher DRGEP cutoff value ($5 * 10^{-4}$ for the ten RII species set vs. $2.5 * 10^{-4}$ for the five RII species set) can induce large error if the ten RII species set remains incompletely filled for many consecutive time steps. For this reason the mass fraction cutoff for this set was lowered to 10^{-10} for this RII target set. The performance of this target species set merits further investigation into the 'scattershot' RII approach; further improvements may come from a more robust method of filtering out biased RII species values, as well as a control strategy that varies the DRGEP cutoff value based on the number of RII target species selected.

4.4 Isopentanol Constant Volume Simulations

Biofuels are attractive possible alternate fuels that can reduce greenhouse gas and pollutant emissions. Isopentanol is one of a variety of next-generation biofuels that may be used as an alternative fuel source for combustion engines. As isopentanol has a volumetric energy density over 30% higher than that of ethanol, and is additionally less hygroscopic it has the capability to be a better alternative fuel for gasoline engines [86]. Isopentanol is a C5 branched alcohol with a methyl branch; as such it exhibits very different chemistry from n-heptane, with minimal NTC behavior and generally undergoing only single stage ignition processes. As such, it is a good choice to further demonstrate the general applicability of the RII method. A 360 species isopentanol mechanism from Sarathy et al. [87] was used in this section to study constant volume ignition under HCCI conditions as well as single cell HCCI simulations adapted from Yang et al. [88].

In Fig. 19, two target species selections with similar maximum error levels (~8%) are compared. The RII method is capable of reproducing the ignition delays over a wide range of initial temperatures and equivalence ratios. The relevant ignition delay error statistics are summarized in Table 5. The normalized wall times of the static target species are slightly faster for most cases.

In Fig. 20, two target species selections with a higher maximum error level (~16%) are compared. Again the RII method is capable of matching the accuracy of the static target species set over the range of the ignition delay curves. The relevant ignition delay error statistics are summarized in Table 6. It is interesting to note that the RII method has the largest error in the high temperature region. For example, if only ignition delay cases with initial temperature less than 1100K are considered, the maximum error of the RII target set drops to 7.92% from 16.01%. For the highest equivalence ratio considered ($\phi = 1$), the ignition delay simulation only runs for 20-60 simulation time steps before ignition in this region, making each time step particularly important to accurate ignition delay predictions. It has been found that decreasing the simulation time step (to 10^{-6}s) can correct this problem, but further investigation is

required to see if the skeletal mechanisms generated by the RII method have a more limited timescale of validity in this region. Again, the normalized wall times of this RII target set are slower for most cases.

4.5 Isopentanol Engine Simulation

In Fig. 21, a comparison of RII and static target simulations of the isopentanol mechanism under HCCI conditions are presented for a single cell engine simulation. Engine conditions were adapted from [88], and are summarized in Table 7. The smaller static target species set (isopentanol, HO_2, CO) was determined based on the target selection criteria proposed by Liang et al. [69], while the larger target species set additionally included OH based on the wider range of applicability of a similar target species set discussed in section 2.5 (Fig. 4).

In Fig. 21 it is seen that all of the target species sets predict the ignition crank angle very well, to within 1.6° for all target species sets. The RII target sets are seen to be considerably more accurate in the prediction of ignition delay. The RII target species set with a higher DRGEP cutoff value (0.05) has similar accuracy to the static target species sets with a lower DRGEP cutoff value (0.01), while the RII target species set with a lower DRGEP cutoff value (0.01) is the only target species set to predict the ignition delay angle to within 1°. The RII target set with a higher DRGEP cutoff value (0.05) evaluates considerably fewer species than the static target species sets, for a similar level of accuracy. For most of the pre-ignition period this RII target set evaluates 20-60 fewer species than the static targets sets, the only exception being immediately prior to ignition, where the static target species sets start evaluating slightly fewer species. Further, even the more accurate RII target set (DRGEP cutoff of 0.01) evaluates fewer species than the static targets for most of the simulation. Finally, the decrease in active species for the target species sets before ignition is the likely cause of their higher error; this may indicate that the static target species sets are no longer valid at that point of the simulation. It is interesting to note that the RII method was capable of similar accuracy in ignition delay predictions compared to static target species sets while generating significantly smaller skeletal mechanisms for both the n-heptane and isopentanol

HCCI engine simulations studied. Further investigation into the computation performance benefits of using the RII method for HCCI conditions is merited.

4.6 Chapter Figures and Tables

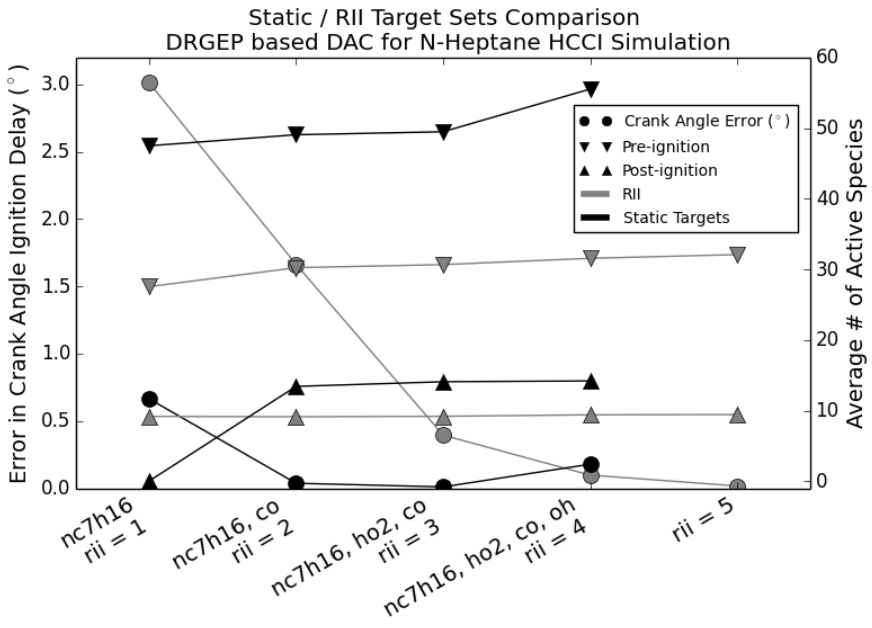

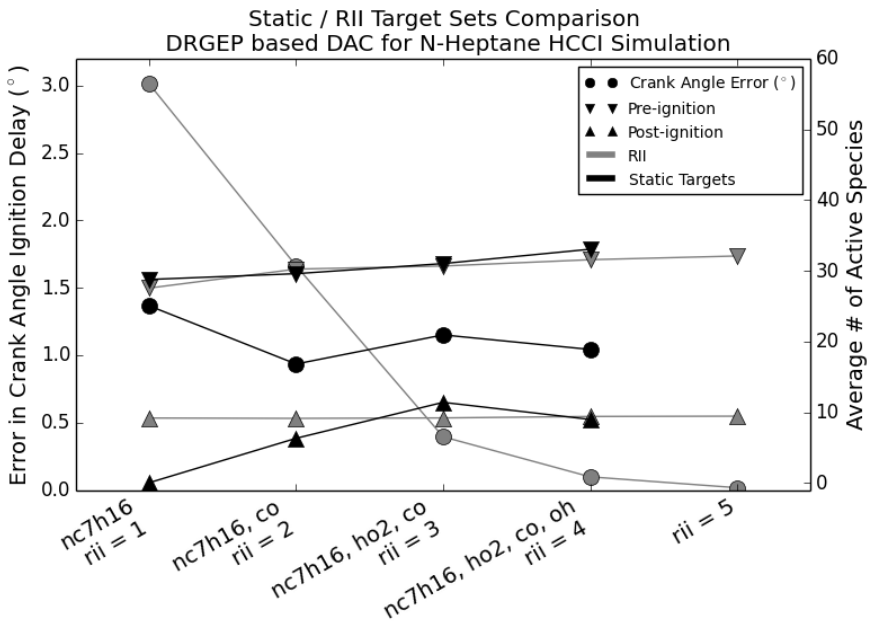

Figure 14: Comparison of DRGEP based DAC simulations of static target sets and RII selected targets for the same HCCI conditions pictured in Fig.3. Static target species were removed from the target species set when their mass fraction was less than 10^{-30}. The species with the maximum 1-5 (corresponding to graph) RII value with mass fraction greater than 10^{-8} were considered for RII targets. Additionally the mass fraction cutoff for OH and HO_2 was lowered to 10^{-15}. Top: The DRGEP cutoff was set to 0.001 for the static target sets and 0.005 for the RII target sets. Bottom: The DRGEP cutoff was set to 0.005 for the static target sets and 0.005 for the RII target sets.

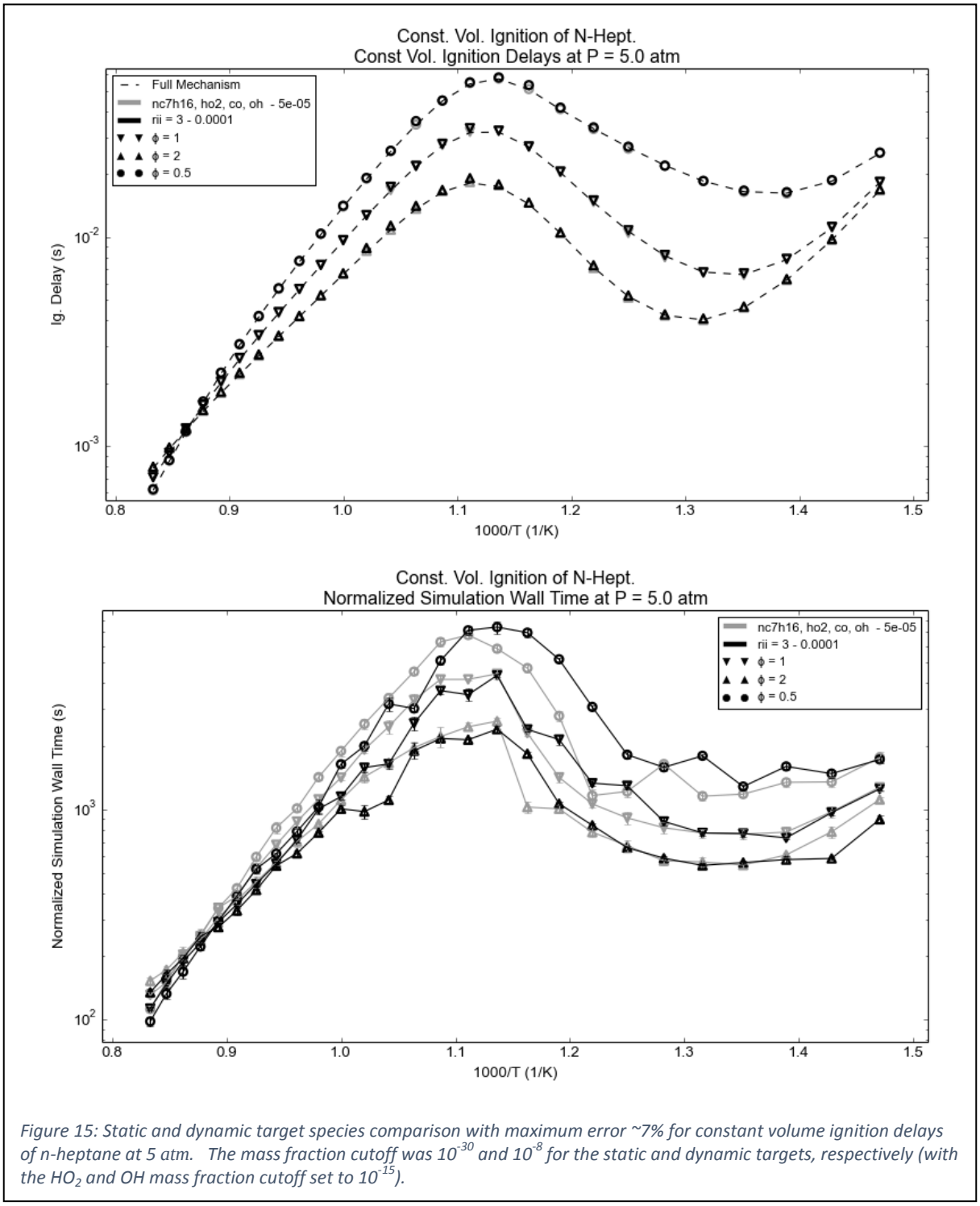

Figure 15: Static and dynamic target species comparison with maximum error ~7% for constant volume ignition delays of n-heptane at 5 atm. The mass fraction cutoff was 10^{-30} and 10^{-8} for the static and dynamic targets, respectively (with the HO_2 and OH mass fraction cutoff set to 10^{-15}).

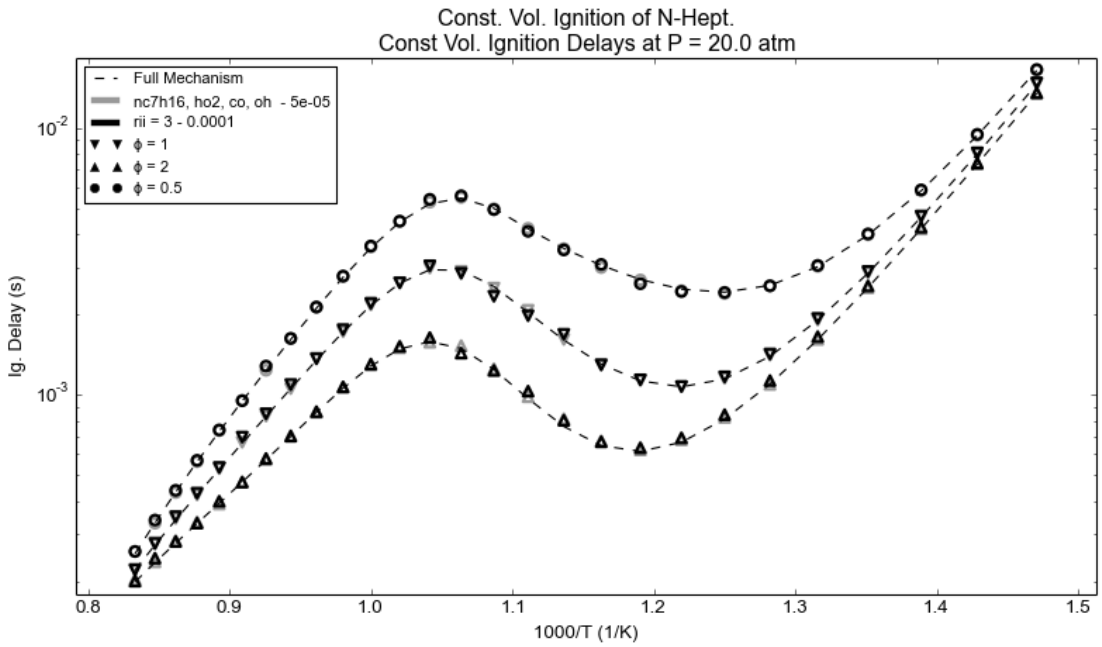

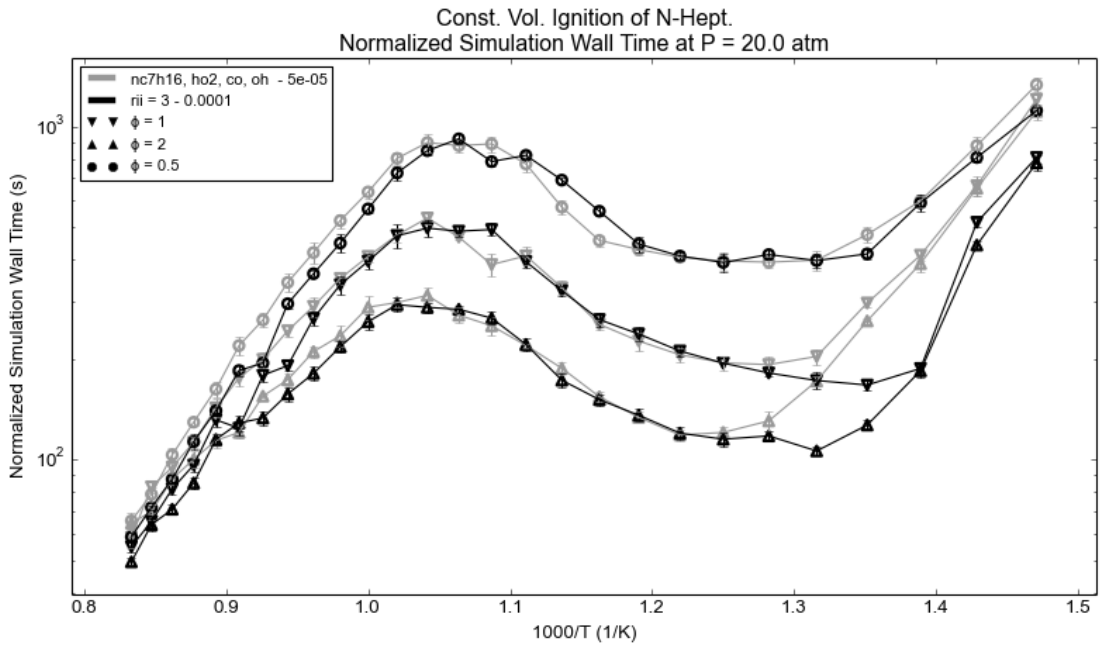

Figure 16: Static and dynamic target species comparison with maximum error ~7% for constant volume ignition delays of n-heptane at 20 atm. The mass fraction cutoff was 10^{-30} and 10^{-8} for the static and dynamic targets, respectively (with the HO_2 and OH mass fraction cutoff set to 10^{-15}).

Table 3: Maximum and Average error for the target species selections in Fig. 15 & 16, as well as the average percent of simulation time spent in the reduction step.

Target Species Set	ε_{DRGEP}	Max % Error:	Avg. % Error:	Avg. % of Time Spent in Reduction:
nc7h16, ho2, co, oh	$5 * 10^{-5}$	6.90	0.71	0.80
rii = 3	10^{-4}	8.11	1.76	0.83

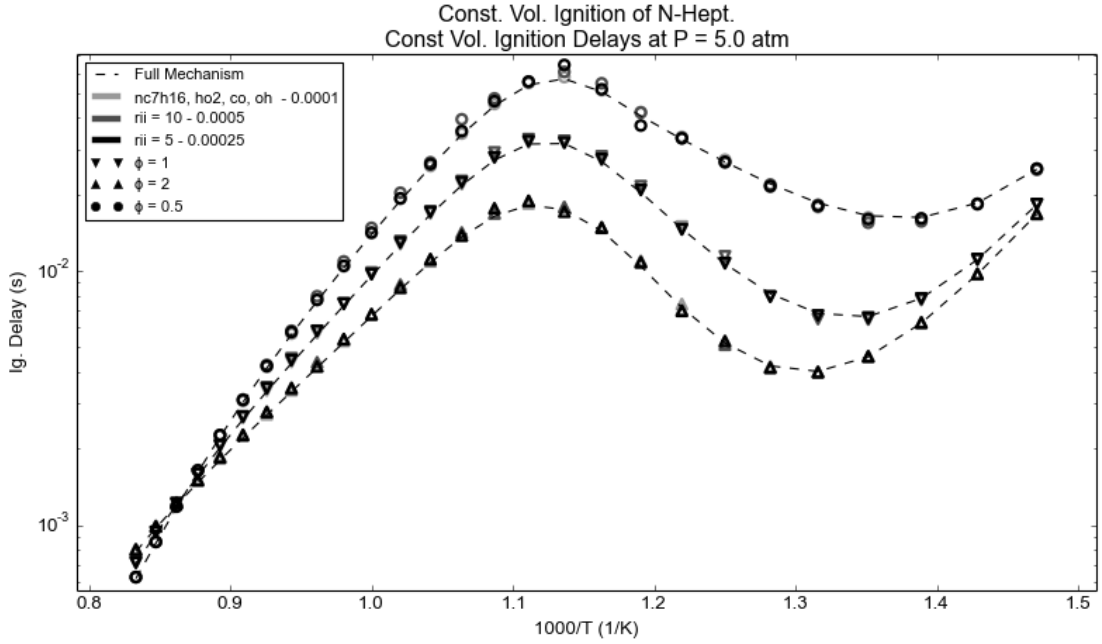

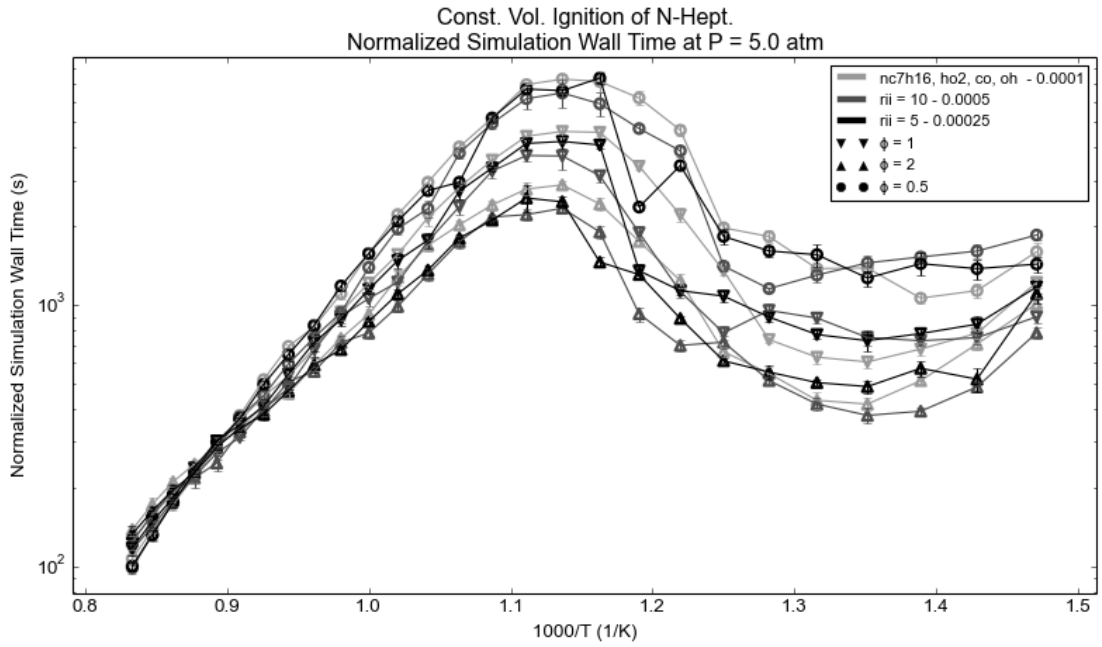

Figure 17: Static and dynamic target species comparison with maximum error ~15% for constant volume ignition delays of n-heptane at 5 atm. The mass fraction cutoff was 10^{-30} static targets set and $10^{-8}/10^{-10}$ for the five and ten RII species target sets respectively (with the HO_2 and OH mass fraction cutoff set to 10^{-15} in both cases).

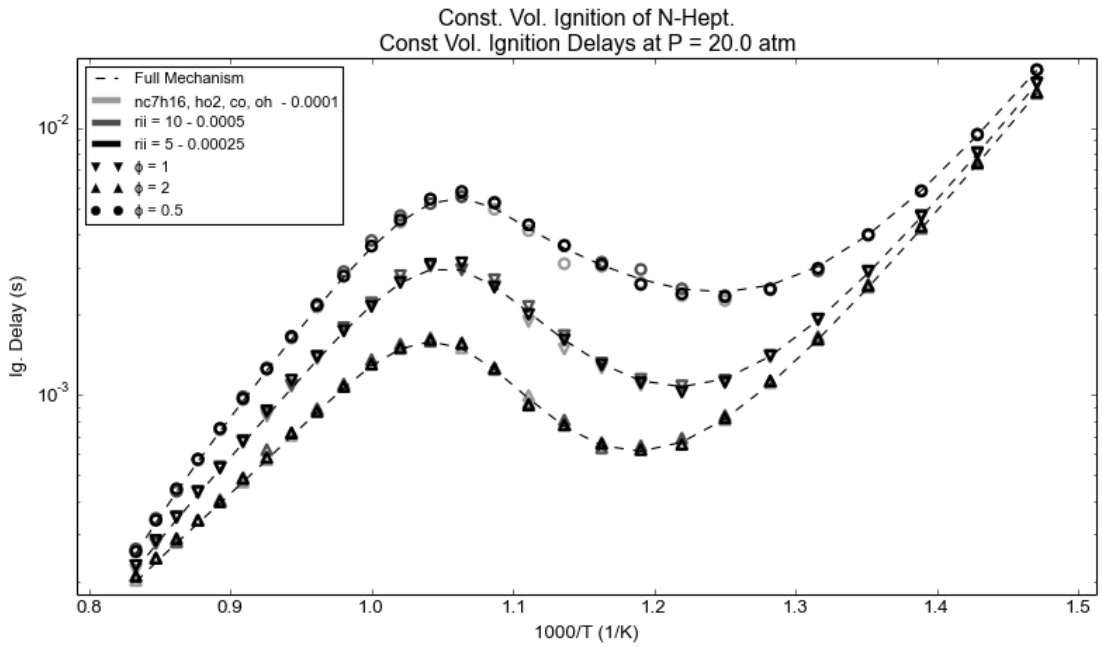

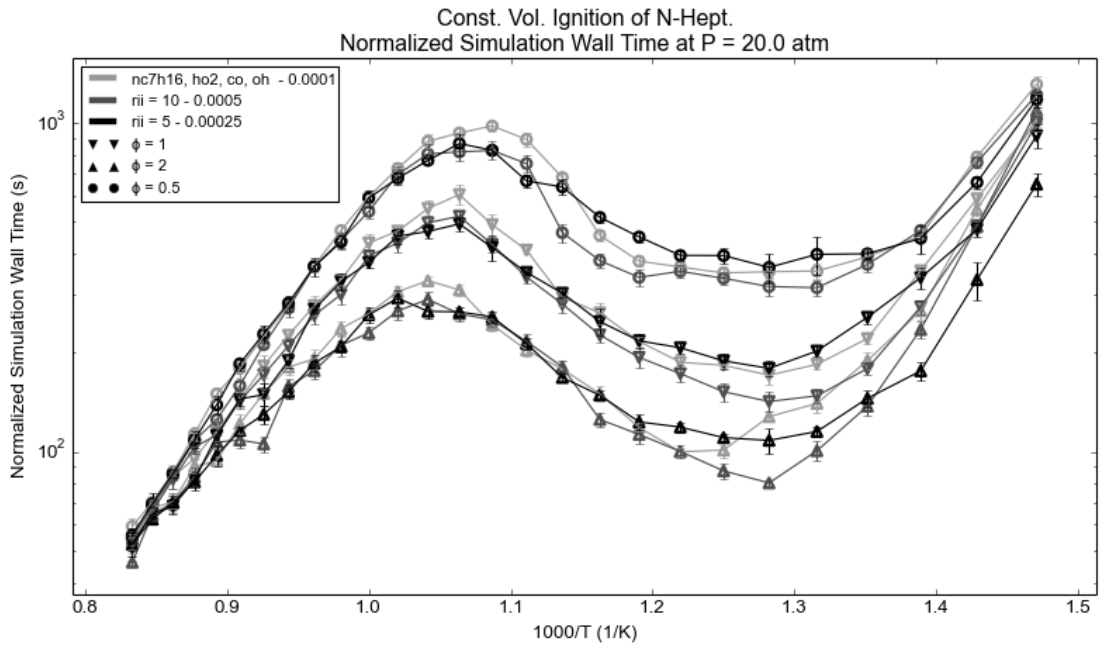

Figure 18: Static and dynamic target species comparison with maximum error ~15% for constant volume ignition delays of n-heptane at 20 atm. The mass fraction cutoff was 10^{-30} static targets set and 10^{-8}/10^{-10} for the five and ten RII target sets, respectively (with the HO_2 and OH mass fraction cutoff set to 10^{-15} in both cases).

Table 4: Maximum and Average error for the target species selections in Fig. 15, as well as the average percent of simulation time spent in the reduction step.

Target Species Set	ε_{DRGEP}	Max % Error:	Avg. % Error:	Avg. % of Time Spent in Reduction:
nc7h16, ho2, co, oh	10^{-4}	12.48	1.58	0.79
rii = 5	$2.5 * 10^{-4}$	13.40	2.20	0.87
rii = 10	$5 * 10^{-4}$	14.85	2.98	0.87

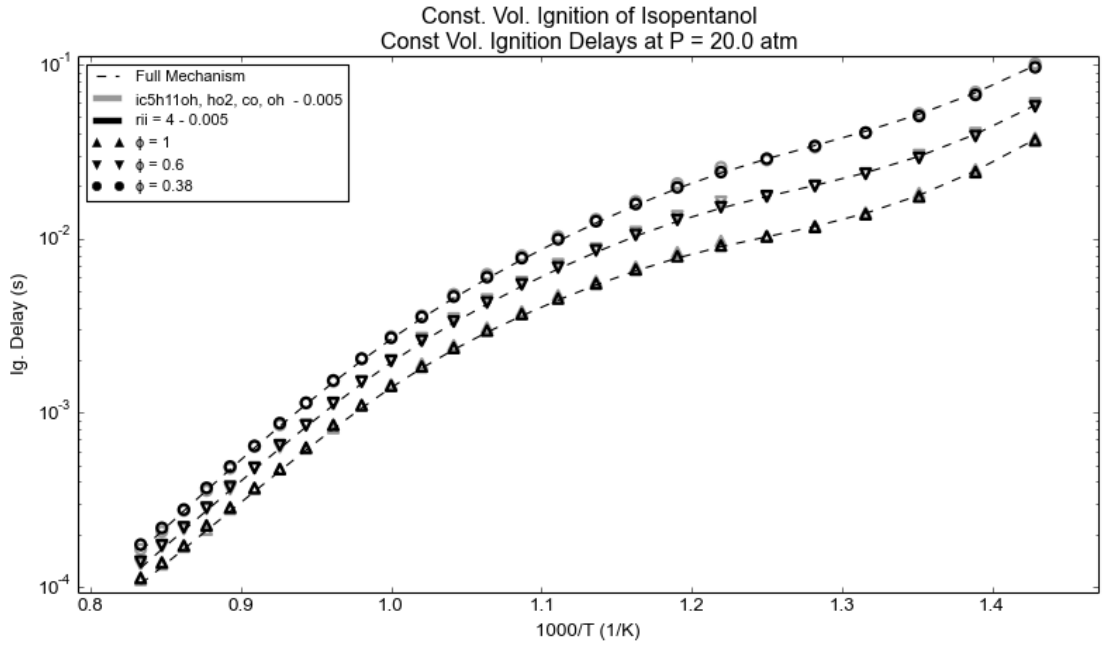

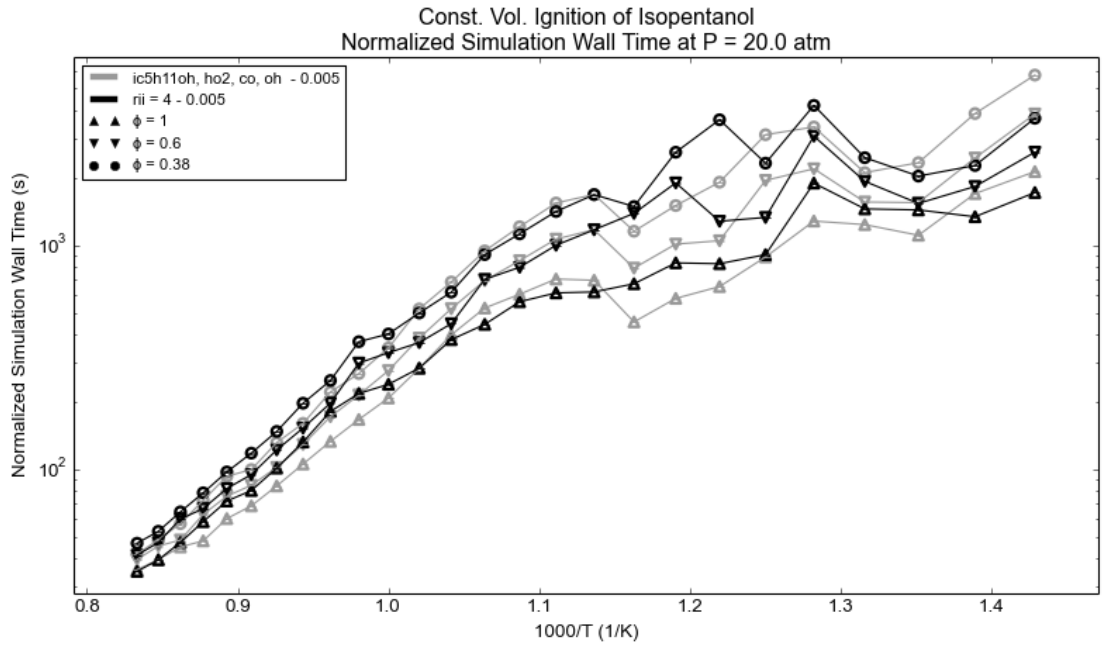

Figure 19: Static and dynamic target species comparison with maximum error ~8% for constant volume ignition delays of isopentanol. The mass fraction cutoff for the static targets was 10^{-30} and 10^{-8} for the dynamic targets (with the HO_2 and OH mass fraction cutoff set to 10^{-15}).

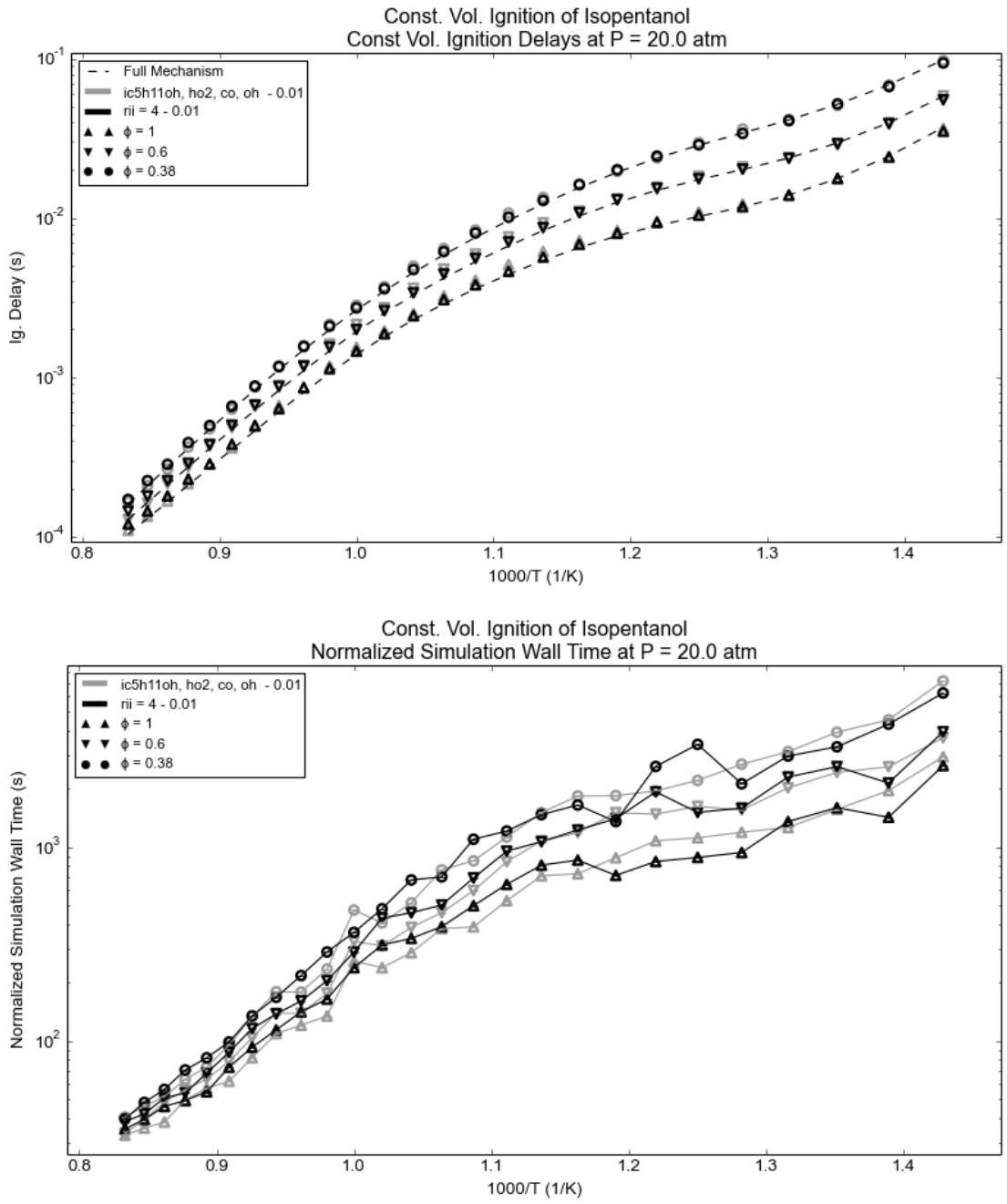

Figure 20: Static and dynamic target species comparison with maximum error ~16% for constant volume ignition delays of isopentanol. The mass fraction cutoff for the static targets was 10^{-30} and 10^{-8} for the dynamic targets (with the HO_2 and OH mass fraction cutoff set to 10^{-15}).

Table 5: Maximum and Average error for the target species selections in Fig. 19, as well as the average percent of simulation time spent in the reduction step.

Target Species Set	ε_{DRGEP}	Max % Error:	Avg. % Error:	Avg. % of Time Spent in Reduction:
ic5h11oh, ho2, co, oh	$5 * 10^{-3}$	8.73	3.48	0.40
rii = 4	$5 * 10^{-3}$	8.66	2.73	0.42

Table 6: Maximum and Average error for the target species selections in Fig. 20, as well as the average percent of simulation time spent in the reduction step.

Target Species Set	ε_{DRGEP}	Max % Error:	Avg. % Error:	Avg. % of Time Spent in Reduction:
ic5h11oh, ho2, co, oh	10^{-2}	15.10	5.65	0.38
rii = 4	10^{-2}	16.01	4.86	0.40

Table 7: Isopentanol engine simulation conditions. Engine properties and initial conditions from [88].

T_0 (K)	405
P_0 (atm)	1
RPM	1200
φ	0.38
Connecting Rod / Crank ratio	3.2
Displacement Volume (L)	0.981
Compression Ratio	14

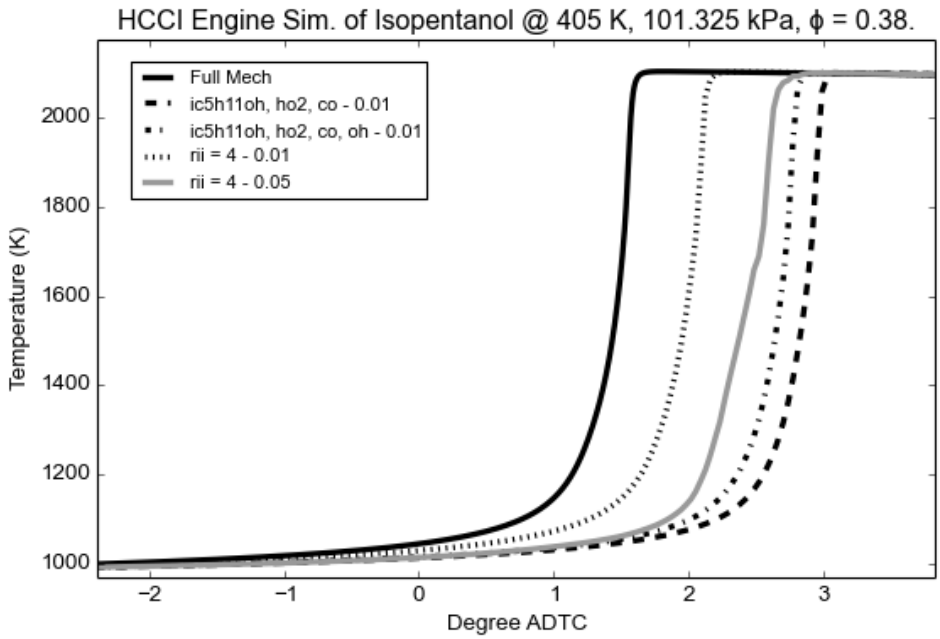

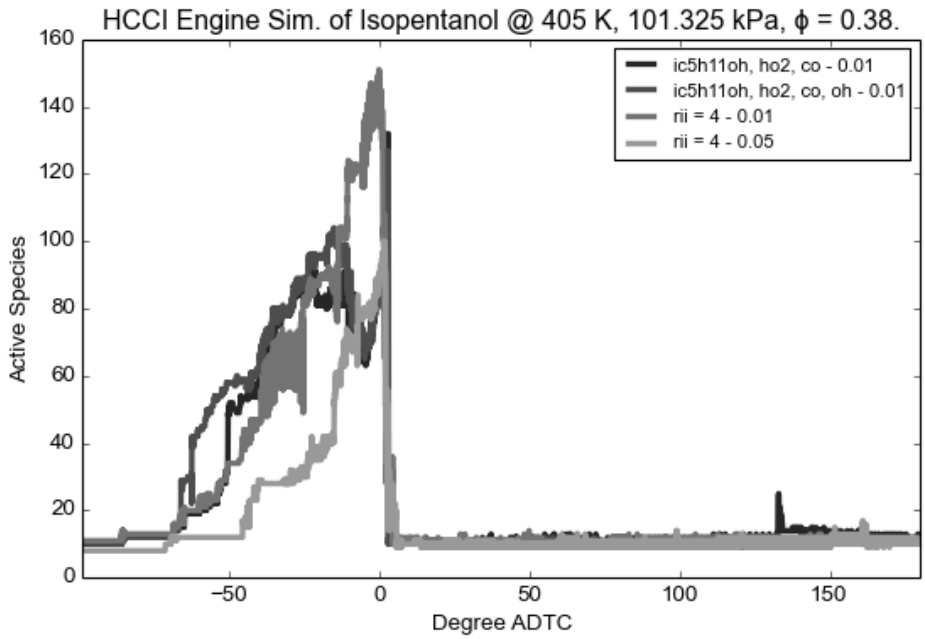

Figure 21: Static and dynamic target species comparison for single cell engine simulation of isopentanol under HCCI conditions. The mass fraction cutoff for the static targets was 10^{-30} and 10^{-8} for the RII sets (with the HO_2 and OH mass fraction cutoff set to 10^{-15}).

5. Conclusions and Further Research

A novel method of determining appropriate target species for DRGEP based DAC simulations was developed and implemented. The Relative Importance Index (RII) method is capable of accurately predicting constant volume ignition delays for a wide variety of conditions for n-heptane [71, 83, 84] and isopentanol [87] detailed mechanisms. Additionally, the RII method was shown to accurately reproduce ignition crank angle delays for single cell engine simulations under HCCI conditions using both mechanisms.

The selection of static target species requires user knowledge of both the combustion mechanism under consideration as well as the important expected combustion processes in order to make appropriate choices of static target species. If improper static target species are selected, or unexpected combustion conditions are encountered, the accuracy and computational efficiency of a DRGEP based DAC method can be drastically impacted. As the RII method determines appropriate target species solely from the local thermochemical state, its use eliminates the concern of static target species sets being applied to inappropriate combustion processes and conditions. Further, as the target selection process is automated, far less prior knowledge on the important combustion processes and target species is required of the user in order to determine an appropriate DRGEP target species set.

It is possible that further parametric studies will continue to demonstrate the improved performance offered by the RII target method. However, it appears that even with dynamically selected target species, there is a minimum size limit in order for skeletal mechanisms generated by the DRGEP method to maintain reasonable accuracy. Going past this limit rapidly induces large amounts of error in combustion target predictions. The result of this is that the speed of DRGEP based DAC simulations using the RII method and static target species sets could be roughly similar for certain combustion simulations, such as the constant volume ignition cases shown in this work. On the other hand, the RII method shows considerable improvement in the HCCI simulations tested suggesting that the RII method may be particularly valuable under HCCI conditions. The ‘scattershot’ RII target set described in section

4.3 seemed to have the best normalized wall times for the n-heptane constant volume simulations with a higher error limit in ignition delay (~15%).

Further improvement to the RII method is likely to be achieved via two avenues. First, more parametric studies of the 'scattershot' RII approach may lead to improved performance; the approach would likely benefit from a more rigorous RII bias detection strategy, as well as by modifying the DRGEP cutoff value based on the number of RII targets considered. Secondly, a method of determining the appropriate DRGEP cutoff value based on the local thermochemical state could prove to be greatly beneficial to the overall speed of DRGEP based DAC simulations. In this work, the DRGEP cutoff values for ignition delay studies were determined such that accuracy is maintained over the entire ignition delay curve. However, if only specific regions of the ignition delay curve are of interest (e.g. the low temperature region) the DRGEP cutoff value can often be relaxed significantly. In addition, for other combustion problems, e.g., in the n-heptane HCCI simulation studied, the DRGEP cutoff value could often be raised by an order of magnitude (compared to the DRGEP cutoff value required for accuracy in n-heptane constant volume ignition studies) while maintaining reasonably accurate predictions of ignition crank angle. Therefore, by varying the DRGEP cutoff with the local thermochemical state, significant speedup may be achieved.

Appendix A

Optimizations for Dynamic Adaptive Chemistry Methods

As alluded to in section 1.3.3.2, several optimizations were made to the graph search method to speed the reduction process. Presented in Fig. 22 below is pseudo-code for the graph search used:

The main advantages of this search are as follows:

1) **All targets are searched together as a set.**

Consider the OIC update step **(4)**. If a species *Node* neighbors one of the target species, then at some point in the while loop, *neighbor* will be a target species. However, the OIC of each target species is set to unity, and thus will not be changed in the OIC update step **(4)**. If *Node* does not neighbor a target species, then the OIC update step will act as if only a single target species is being searched. Searching the targets together as a set effectively makes the search more efficient for multiple targets.

2) **All edges with DRGEP coefficient smaller than the DRGEP cutoff are not expanded**

Say $r\_AB[node, neighbor] < \varepsilon_{DRGEP}$, for a given node and neighbor. This implies that if $R[node] * r\_AB[node, neighbor] < \varepsilon_{DRGEP}$. Therefore the OIC value of all possible paths traveling through 'node' to 'neighbor' will be less than the DRGEP cutoff, and will not be updated in **(4)**; any species further along this path will therefore will not be included in the skeletal mechanism if it not included through an alternative path. Therefore it is safe to ignore this edge. This is similar to the RBFS algorithm presented by Liang et al [68].

3) **Once the maximum queued OIC value is less than the DRGEP cutoff, the search can be ended**

Following from 2), if the maximum OIC value remaining is less than the DRGEP cutoff, than no updates to the OIC array after this point in the search can result in a OIC greater than the DRGEP

cutoff (i.e. no new species will be added to the skeletal mechanism). Therefore we can end the search.

```
//Arguments:
//      targets – the list of target species to use in the search
//      r_AB    – the DRG coefficient matrix
//      R       – output array storing the OICs
//      ε_DRGEP – the DRGEP cutoff
Optimized_Dijkstras_Search (targets, r_AB, R, ε_DRGEP)
{
        Set R = 0
        nodes_to_visit = {all species}
1)      Foreach target in targets
                Set R[target] = 1
        next_node = targets[0]
        While (nodes_to_visit is not empty)
        {
                Node = nodes_to_visit[next_node]
                Erase next_node from nodes_to_visit
3)              If (R[Node] < ε_DRGEP)
                        Exit
                Foreach neighbor of Node
                {
2)                      If (r_AB[Node, neighbor] < ε_DRGEP)
                                Continue
4)                      R[neighbor] = max(R[neighbor], R[Node] * r_AB[Node, neighbor])
                }
                next_node = index of node in nodes_to_visit with maximum R[node]
        }
}
```

Figure 22: Pseudo code of the optimized Dijkstra's search

References

1. U. S. E. I. Administration Energy sources have changed throughout the history of the United States. http://www.eia.gov/todayinenergy/detail.cfm?id=11951
2. U. S. E. I. Administration Emissions of Greenhouse Gases in the U. S. http://www.eia.gov/environment/emissions/ghg_report/ghg_carbon.cfm
3. M. L. f. E. a. t. Environment, in: Cambridge, Massachusetts, 2008.
4. A. Krein; G. Williams, Innovation for Sustainable Aviation in a Global Environment: Proceedings of the Sixth European Aeronautics Days (2012) 63
5. A. Bhagatwala; J. H. Chen; T. Lu, Combustion and Flame) http://dx.doi.org/10.1016/j.combustflame.2013.12.027.
6. M. C. Drake; D. C. Haworth, Proceedings of the Combustion Institute 31 (1) (2007) 99-124 http://dx.doi.org/10.1016/j.proci.2006.08.120.
7. K. He; I. P. Androulakis; M. G. Ierapetritou, Energy & Fuels 25 (8) (2011) 3369-3376 10.1021/ef200290z.
8. N. P. Komninos; C. D. Rakopoulos, Renewable and Sustainable Energy Reviews 16 (3) (2012) 1588-1610 http://dx.doi.org/10.1016/j.rser.2011.11.026.
9. S. Visakhamoorthy; T. Tzanetakis; D. Haggith; A. Sobiesiak; J. Z. Wen, Applied Energy 92 (2012) 437-446 http://dx.doi.org/10.1016/j.apenergy.2011.11.014.
10. H. Cheng; Y. Changjin; M. G. Rohan; A. William; S. Venke, in: 52nd Aerospace Sciences Meeting, American Institute of Aeronautics and Astronautics: 2014.
11. A. Kumud; M. Hukam; L. Phil, in: 51st AIAA Aerospace Sciences Meeting including the New Horizons Forum and Aerospace Exposition, American Institute of Aeronautics and Astronautics: 2013.
12. S. M. Correa, Proceedings of the Combustion Institute 27 (2) (1998) 1793-1807
13. T. Lu; C. K. Law, Progress in Energy and Combustion Science 35 (2) (2009) 192-215
14. T. W. A. F. Zhao, D.N. Assanis, J.E. Dec, J.A. Eng, P.M. Najt, SAE International (2003)
15. M. Yao; Z. Zheng; H. Liu, Progress in Energy and Combustion Science 35 (5) (2009) 398-437 http://dx.doi.org/10.1016/j.pecs.2009.05.001.
16. W. Meier; X. R. Duan; P. Weigand, Combustion and Flame 144 (1–2) (2006) 225-236 http://dx.doi.org/10.1016/j.combustflame.2005.07.009.
17. W. Polifke; D. G. Nicol; P. C. Malte; K. Döbbeling; T. Sattelmayer, Journal of Engineering for Gas Turbines and Power 118 (4) (1996) 765-772 10.1115/1.2816992.
18. S. J. Shanbhogue; S. Husain; T. Lieuwen, Progress in Energy and Combustion Science 35 (1) (2009) 98-120 http://dx.doi.org/10.1016/j.pecs.2008.07.003.
19. M. Mehl; W. J. Pitz; C. K. Westbrook; H. J. Curran, Proceedings of the Combustion Institute 33 (1) (2011) 193-200 http://dx.doi.org/10.1016/j.proci.2010.05.027.
20. O. Herbinet; W. J. Pitz; C. K. Westbrook, Combustion and Flame 157 (5) (2010) 893-908 http://dx.doi.org/10.1016/j.combustflame.2009.10.013.
21. S. R. Tonse; N. W. Moriarty; M. Frenklach; N. J. Brown, International Journal of Chemical Kinetics 35 (9) (2003) 438-452
22. L. Liang; S.-C. Kong; C. Jung; R. D. Reitz, Journal of Engineering for Gas Turbines and Power 129 (1) (2007) 271-278
23. Y. Shi; L. Liang; H.-W. Ge; R. D. Reitz, Combustion Theory and Modelling 14 (1) (2010) 69-89 10.1080/13647830903548834.
24. I. G. Zsély; T. Turányi, Physical Chemistry Chemical Physics 5 (17) (2003) 3622-3631
25. D. Leonard Chapman; L. Kingsley Underhill, Journal of the Chemical Society, Transactions 103 (1913) 496-508

26. J. D. Ramshaw, Physics of Fluids 23 (4) (1980) 675
27. S. W. Benson, The Journal of Chemical Physics 20 (10) (1952) 1605-1612 doi:http://dx.doi.org/10.1063/1.1700223.
28. S. Lam, Combustion Science and Technology 89 (5-6) (1993) 375-404
29. S. Lam; D. Coussis, Proceedings of the Combustion Institute 22 (1) (1989) 931-941
30. S. Lam; D. Goussis, International Journal of Chemical Kinetics 26 (4) (1994) 461-486
31. U. Maas; S. B. Pope, Combustion and Flame 88 (3) (1992) 239-264
32. T. Lu; Y. Ju; C. K. Law, Combustion and Flame 126 (1) (2001) 1445-1455
33. T. Lu; C. K. Law, Combustion and Flame 154 (4) (2008) 761-774
34. H. Rabitz; M. Kramer; D. Dacol, Annual review of physical chemistry 34 (1) (1983) 419-461
35. T. Turanyi, New Journal of Chemistry 14 (11) (1990) 795-803
36. T. Turányi, Journal of Mathematical Chemistry 5 (3) (1990) 203-248
37. S. Vajda; P. Valko; T. Turanyi, International Journal of Chemical Kinetics 17 (1) (1985) 55-81
38. J. Prager; H. N. Najm; M. Valorani; D. A. Goussis, Proceedings of the Combustion Institute 32 (1) (2009) 509-517
39. M. Valorani; F. Creta; F. Donato; H. N. Najm; D. A. Goussis, Proceedings of the Combustion Institute 31 (1) (2007) 483-490
40. M. Valorani; F. Creta; D. A. Goussis; J. C. Lee; H. N. Najm, Combustion and Flame 146 (1) (2006) 29-51
41. T. Løvås, Combustion and Flame 156 (7) (2009) 1348-1358
42. T. Løvås; P. Amnéus; F. Mauss; E. Mastorakos, Proceedings of the Combustion Institute 29 (1) (2002) 1387-1393
43. T. Løvås; F. Mauss; C. Hasse; N. Peters, Proceedings of the Combustion Institute 29 (1) (2002) 1403-1410
44. T. Løvas; D. Nilsson; F. Mauss, Proceedings of the Combustion Institute 28 (2) (2000) 1809-1815
45. K. Edwards; T. Edgar; V. Manousiouthakis, Computers & chemical engineering 22 (1) (1998) 239-246
46. L. Elliott; D. Ingham; A. Kyne; N. Mera; M. Pourkashanian; C. Wilson, Progress in Energy and Combustion Science 30 (3) (2004) 297-328
47. B. Bhattacharjee; D. A. Schwer; P. I. Barton; W. H. Green, Combustion and Flame 135 (3) (2003) 191-208
48. O. O. Oluwole; B. Bhattacharjee; J. E. Tolsma; P. I. Barton; W. H. Green, Combustion and Flame 146 (1) (2006) 348-365
49. A. Mitsos; G. M. Oxberry; P. I. Barton; W. H. Green, Combustion and Flame 155 (1) (2008) 118-132
50. T. Lu; C. K. Law, Proceedings of the Combustion Institute 30 (1) (2005) 1333-1341
51. T. Lu; C. K. Law, Combustion and Flame 144 (1–2) (2006) 24-36 http://dx.doi.org/10.1016/j.combustflame.2005.02.015.
52. T. Lu; C. K. Law, Combustion and Flame 154 (1–2) (2008) 153-163 http://dx.doi.org/10.1016/j.combustflame.2007.11.013.
53. P. Pepiot-Desjardins; H. Pitsch, Combustion and Flame 154 (1–2) (2008) 67-81 http://dx.doi.org/10.1016/j.combustflame.2007.10.020.
54. M. Raju; C. Sung; K. Kundu in: *Integrating sensitivity analysis into directed relation graph with error propagation for effective chemical mechanism reduction*, Fall Technical Meeting of the Eastern States Section of the Combustion Institute, number A-26, 2007; 2007.
55. K. E. Niemeyer; C.-J. Sung; M. P. Raju, Combustion and Flame 157 (9) (2010) 1760-1770 http://dx.doi.org/10.1016/j.combustflame.2009.12.022.

56. T. Lu; C. K. Law, Combustion and Flame 146 (3) (2006) 472-483 http://dx.doi.org/10.1016/j.combustflame.2006.04.017.
57. K. E. Niemeyer; C.-J. Sung, Combustion and Flame 158 (8) (2011) 1439-1443 http://dx.doi.org/10.1016/j.combustflame.2010.12.010.
58. H. Huang; M. Fairweather; J. F. Griffiths; A. S. Tomlin; R. B. Brad, Proceedings of the Combustion Institute 30 (1) (2005) 1309-1316 http://dx.doi.org/10.1016/j.proci.2004.08.001.
59. G. Li; H. Rabitz, Chemical Engineering Science 44 (6) (1989) 1413-1430 http://dx.doi.org/10.1016/0009-2509(89)85014-6.
60. P. Pepiot-Desjardins; H. Pitsch, Combustion Theory and Modelling 12 (6) (2008) 1089-1108 10.1080/13647830802245177.
61. Z. Luo; M. Plomer; T. Lu; S. Som; D. E. Longman; S. M. Sarathy; W. J. Pitz, Fuel 99 (0) (2012) 143-153 http://dx.doi.org/10.1016/j.fuel.2012.04.028.
62. D. A. Schwer; P. Lu; W. H. Green Jr, Combustion and Flame 133 (4) (2003) 451-465 http://dx.doi.org/10.1016/S0010-2180(03)00045-2.
63. I. Banerjee; M. G. Ierapetritou, Combustion and Flame 144 (3) (2006) 619-633 http://dx.doi.org/10.1016/j.combustflame.2005.10.001.
64. G. P. Smith; D. M. Golden; M. Frenklach; N. W. Moriarty; B. Eiteneer; M. Goldenberg; C. T. Bowman; R. K. Hanson; S. Song; W. C. Gardiner Jr GRI-Mech 3.0. http://www.me.berkeley.edu/gri_mech/
65. K. He; M. G. Ierapetritou; I. P. Androulakis, Combustion and Flame 155 (4) (2008) 585-604 http://dx.doi.org/10.1016/j.combustflame.2008.05.004.
66. Y. Liang; V. Hiremath; S. Pope; P. Pepiot, in: *8th US National Combustion Meeting*, University of Utah, 2013.
67. L. Liang; J. Stevens; J. Farrell; P. Huynh; I. Androulakis; M. Ierapetritou in: *An adaptive approach for coupling detailed chemical kinetics and multidimensional CFD*, 5th US Combustion Meeting, University of California at San Diego, 2007; 2007; pp 25-28.
68. L. Liang; J. G. Stevens; J. T. Farrell, Proceedings of the Combustion Institute 32 (1) (2009) 527-534 http://dx.doi.org/10.1016/j.proci.2008.05.073.
69. L. Liang; J. G. Stevens; S. Raman; J. T. Farrell, Combustion and Flame 156 (7) (2009) 1493-1502 http://dx.doi.org/10.1016/j.combustflame.2009.02.008.
70. K. He; I. P. Androulakis; M. G. Ierapetritou, Chemical Engineering Science 65 (3) (2010) 1173-1184 http://dx.doi.org/10.1016/j.ces.2009.09.073.
71. H. J. Curran; P. Gaffuri; W. J. Pitz; C. K. Westbrook, Combustion and Flame 114 (1–2) (1998) 149-177 http://dx.doi.org/10.1016/S0010-2180(97)00282-4.
72. P. Brown; G. Byrne; A. Hindmarsh, SIAM Journal on Scientific and Statistical Computing 10 (5) (1989) 1038-1051 10.1137/0910062.
73. J. C. G. Andrae; P. Björnbom; R. F. Cracknell; G. T. Kalghatgi, Combustion and Flame 149 (1–2) (2007) 2-24 http://dx.doi.org/10.1016/j.combustflame.2006.12.014.
74. J. C. G. Andrae; T. Brinck; G. T. Kalghatgi, Combustion and Flame 155 (4) (2008) 696-712 http://dx.doi.org/10.1016/j.combustflame.2008.05.010.
75. H. Yang; Z. Ren; T. Lu; G. M. Goldin, Combustion Theory and Modelling 17 (1) (2012) 167-183 10.1080/13647830.2012.733825.
76. H. Wang; X. You; A. Joshi; S. Davis; A. Laskin; F. Egolfopoulos; C. Law USC Mech Version II. High-Temperature Combustion Reaction Model of H 2/CO/C 1–C 4 Compounds, May 2007. http://ignis.usc.edu/USC_Mech_II.htm
77. L. Tosatto; B. A. V. Bennett; M. D. Smooke, Combustion and Flame 160 (9) (2013) 1572-1582 http://dx.doi.org/10.1016/j.combustflame.2013.03.024.

78. X. Gou; Z. Chen; W. Sun; Y. Ju, Combustion and Flame 160 (2) (2013) 225-231 http://dx.doi.org/10.1016/j.combustflame.2012.10.015.
79. W. Sun; Z. Chen; X. Gou; Y. Ju, Combustion and Flame 157 (7) (2010) 1298-1307 http://dx.doi.org/10.1016/j.combustflame.2010.03.006.
80. Y. Shi; R. P. Hessel; R. D. Reitz, Combustion Theory and Modelling 13 (1) (2009) 83-104 10.1080/13647830802401101.
81. Dave Goodwin; Nicholas Malaya; Harry Moffat; R. Speth Cantera. An object-oriented software toolkit for chemical kinetics, thermodynamics, and transport processes. Version 2.1a1. https://code.google.com/p/cantera/
82. N. Peters; G. Paczko; R. Seiser; K. Seshadri, Combustion and Flame 128 (1–2) (2002) 38-59 http://dx.doi.org/10.1016/S0010-2180(01)00331-5.
83. H. J. Curran; P. Gaffuri; W. J. Pitz; C. K. Westbrook, Combustion and Flame 129 (3) (2002) 253-280
84. LLNL n-Heptane, Detailed Mechanism, Version 2. https://www-pls.llnl.gov/?url=science_and_technology-chemistry-combustion-nc7h16
85. M. Sjöberg; J. E. Dec; W. Hwang, in: SAE Technical Paper 2007-01-0207: 2007.
86. T. Tsujimura; W. J. Pitz; F. Gillespie; H. J. Curran; B. W. Weber; Y. Zhang; C.-J. Sung, Energy & Fuels 26 (8) (2012) 4871-4886 10.1021/ef300879k.
87. S. Mani Sarathy; S. Park; B. W. Weber; W. Wang; P. S. Veloo; A. C. Davis; C. Togbe; C. K. Westbrook; O. Park; G. Dayma, Combustion and Flame 160 (12) (2013) 2712-2728
88. Y. Yang; J. Dec; N. Dronniou; B. Simmons, SAE International Journal of Fuels and Lubricants 3 (2) (2010) 725-741